Available online at www.sciencedirect.com
SCIENCE DIRECT®
Journal of African Earth Sciences 40 (2004) 61–79
Journal of African Earth Sciences
www.elsevier.com/locate/jafrearsci

TTG magmatism in the Congo craton; a view from major and trace element geochemistry, Rb–Sr and Sm–Nd systematics: case of the Sangmelima region, Ntem complex, southern Cameroon

C.K. Shang [a,b,*], M. Satir [b], W. Siebel [b], E.N. Nsifa [a], H. Taubald [b], J.P. Liégeois [c], F.M. Tchoua [a]

[a] Department of Earth Sciences, University of Yaounde I, BP 812, Yaounde, Cameroon
[b] Institute of Geosciences, University of Tuebingen, D-72074, Germany
[c] Isotope Geology Section, Central Africa Museum, B-3080 Tervuren, Belgium

Received 21 November 2002; accepted 14 July 2004
Available online 25 September 2004

Abstract

TTG rocks of the Sangmelima region (Ntem complex, Congo craton) in southern Cameroon range in modal composition from rocks of the charnockitic suite, tonalites to granodiorites. They display a wide spectrum of SiO_2 composition (54–76 wt%), including metaluminous intermediate rocks ($0.56 < A/CNK < 1$) and rocks that are slightly peraluminous ($1 < A/CNK < 1.08$). Charnockites and tonalites define a trondhjemitic suite while granodiorites portray a slight potassic calc-alkaline affinity. The primordial mantle-normalized spidergrams are characterized by negative Nb–Ta anomalies, suggesting a subduction related signature or melting of crustal rocks that were formed along subduction zones. More siliceous members of the rock suites are enriched in LILE. REE fractionation is shown by $2 < La_N/Yb_N < 28$ in the charnockitic suite while higher ratios of $12 < La_N/Yb_N < 114$ in the tonalitic suite and $18 < La_N/Yb_N < 99$ in granodiorites indicate melting of source rocks with garnet as a restite phase. Samples with overall lowest abundance in REE show a positive Eu anomaly and represent small amounts of magmas derived from a source with much feldspar contribution to the melt. Sr and Nd systematics coupled with Mg#–SiO_2 compositions are consistent with derivation by partial melting in a subduction setting or merely from a thickened Archaean crust of eclogite facies basaltic proto-crust with mantle material input. From Rb–Sr and Sm–Nd whole-rock data, intrusion timing is defined around 2900 Ma for rocks of the charnockitic suite. The Rb–Sr system in biotite portrays post-emplacement reheating during the Eburnean orogeny. TTG intrusions in the Sangmelima region represent a major Archaean accretion event in the Congo craton.

Keywords: TTG; Subduction; Thickened Archaean crust; Congo craton

1. Introduction

Due to identical chemical characteristics between recent adakitic rocks and Phanerozoic Na-rich granitoids of known tectonic setting, much has been unraveled about ancient TTG (tonalite–trondhjemite–granodiorite) rock formations common in Archaean terrains and of hitherto doubtful origin. An understanding of their origin is therefore essential to comprehend the development of Archaean continental cratons. Over the years, geologists have employed several techniques to study cratonic areas (e.g. Baltic shield, Pilbara craton etc.), and many models have therefore been proposed to account for Archaean crust composition and petrogenesis

* Corresponding author. Address: Institut fur Geowissenschaften, AB Mineralogie und Geodynamik, Eberhard-Karls-Universitat, Wilhelmtrasse 56, D-72074 Tuebingen, Germany. Fax: +49 07071 29 5713.
E-mail addresses: shang004@yahoo.com, cosmas@uni-tuebingen.de (C.K. Shang).

0899-5362/$ - see front matter © 2004 Elsevier Ltd. All rights reserved.
doi:10.1016/j.jafrearsci.2004.07.005

(e.g. Arth and Hanson, 1975; Tarney et al., 1976; Windley, 1976; Barker, 1979; Condie, 1980, 1981; Arndt, 1983; Nisbet and Fowler, 1983; Abbott and Hofmann, 1984; Martin, 1987a,b; Nédélec et al., 1990; Frost et al., 2000). So far, fairly little is known about the Congo craton. Although the Archaean Ntem complex of the Congo craton has been investigated since colonial times, detailed study of the area started only within the context of the SW Cameroon project piloted by BRGM (1975). Using major, trace element and REE geochemical data, Nédélec et al. (1990) presented the first modern results on the Ntem complex in an attempt at addressing the petrogenesis of the Ntem crust. Shang (2001) like Tchameni (1997), proposed the first Archaean and Palaeoproterozoic timings for crustal evolution history of the Ntem complex, where charnockitic rocks form the greater part of the trondhjemitic TTG suite together with rocks of the tonalitic suite, while granodiorites show potassic calc-alkaline affinities. As is the case with other TTG complexes elsewhere, it could be inferred that the Ntem complex TTG were formed in a convergent plate margin, as chemically similar Cenozoic adakites are created from subducted young and hot oceanic crust at pressures high enough to stabilize garnet ± amphibole (e.g. Defant and Drummond, 1990). In fact, it is widely argued that TTG is the Archaean subduction related analogue of adakite (e.g. Drummond and Defant, 1990; Drummond et al., 1996; Martin, 1999). However, similarities with Phanerozoic Na-rich granitoids that represent partial melts of hydrated basaltic material at the base of thickened crust (e.g. Atherton and Pertford, 1993; Muir et al., 1995; Petford and Atherton, 1996; Johnson et al., 1997), suggest that subduction may not be the only possible tectonic setting for TTG.

In this study, we describe the Sangmelima Archaean TTG suite of undisputable igneous origin but that do not share the chemical characteristics of A-type magma as defined by Kilpatrick and Ellis (1992). We also compare Ntem TTG with adakites and high-Mg diorites from other cratonic areas, in an attempt to determine the petrogenesis and tectonic setting and better comprehend Archaean crustal evolution in the Ntem complex. We also use major and trace elements, Sm–Nd and Rb–Sr isotope systematics to show similar source trends for Sangmelima TTG suite, which we interpret as melts from eclogitised basaltic or amphibolitic sources. In addition, Rb–Sr biotite systematics is used to constrain the timing of post-emplacement tectonothermal events on the Ntem complex.

2. Geological setting

The Ntem Complex represents the north-western part of the Archaean Congo craton in Central Africa (e.g. Clifford and Gass, 1970; Cahen et al., 1976; Bessoles and Trompette, 1980) and is very well exposed in southern Cameroon (Rocci, 1965; Maurizot et al., 1985; Goodwin, 1991; Fig. 1). It is limited to the north by a major thrust that marks the contact with the Pan-African orogenic belt (Yaounde group) and is composed of various rock types, with rocks of the TTG suite constituting the greater part (e.g. Nédélec et al., 1990). Three main rock types, the charnockitic suite, granodioritic suite and the tonalitic suite, distinguished on cartographic ground and field observation, make up this TTG unit. The tonalitic suite (known as "Soo granite" in Champetier de Ribes and Aubaque, 1956; and as "Soo tonalite" in Nédélec et al., 1990) is essentially exposed to the north and is strongly mylonitized and retrogressed along the fault boundary with the Pan-African orogenic belt, while granodioritic suite massifs form distinct bodies within the dominantly charnockitic southern zone (Fig. 1). The S_0 structural surface is basically NW–SE in the charnockitic suite, NNE–SSW to almost E–W in the tonalitic suite and E–W to WNW–ESE in granodiorites, indicating structural discordances and suggesting a polyphase structural set-up in the Sangmelima TTG (Shang, 2001). Furthermore, charnockitic xenoliths occur in granodioritic and tonalitic massifs and the latter form veins and dykes in charnockite thus portraying relative chronology for the three members of the TTG suite. Exposures of supracrustal rocks (banded iron formations and sillimanite-bearing paragneisses) that represent remnants of greenstone belts form xenoliths in TTG suite rocks (e.g. Nsifa et al., 1993). Late- to post-tectonic granitoids and syenites with alkaline affinity intrude the TTG (e.g. Kornprobst et al., 1976; Nédélec, 1990; Tchameni, 1997; Tchameni et al., 2000, 2001; Shang, 2001; Shang et al., 2001a,b), and clearly postdate the major crustal forming episode. Eburnean (≈2.1 Ga) doleritic dykes (e.g. Toteu et al., 1994; Vicat et al., 1996) represent the last magmatic activity in the Ntem complex.

Petro-structural studies suggest two major episodes of deformation in this geological domain. The first deformation episode is characterized by vertical foliation, stretching and vertical lineation and isoclinal folds. These structural elements could mark the diapiric emplacement of the granitoids (Shang, 2001; Tchameni et al., 2001). The second major tectonothermal event is marked by the development of sinistral shear planes trending north–south to N45°E, and partial melting of charnockitic and tonalitic members of the TTG suite and the greenstone belt country rocks, described as post-Archaean and post-charnockitic migmatisation by Nsifa and Riou (1990). Although the timing to this second tectonothermal event is not well known, Rb–Sr whole-rock data from Lasserre and Soba (1976) suggest that this event could have occurred during the Eburnean orogeny. Toteu et al. (1994) dated the peak of this metamorphism at about 2050 Ma, using U–Pb zircon data on metamorphic rocks from the Nyong series.

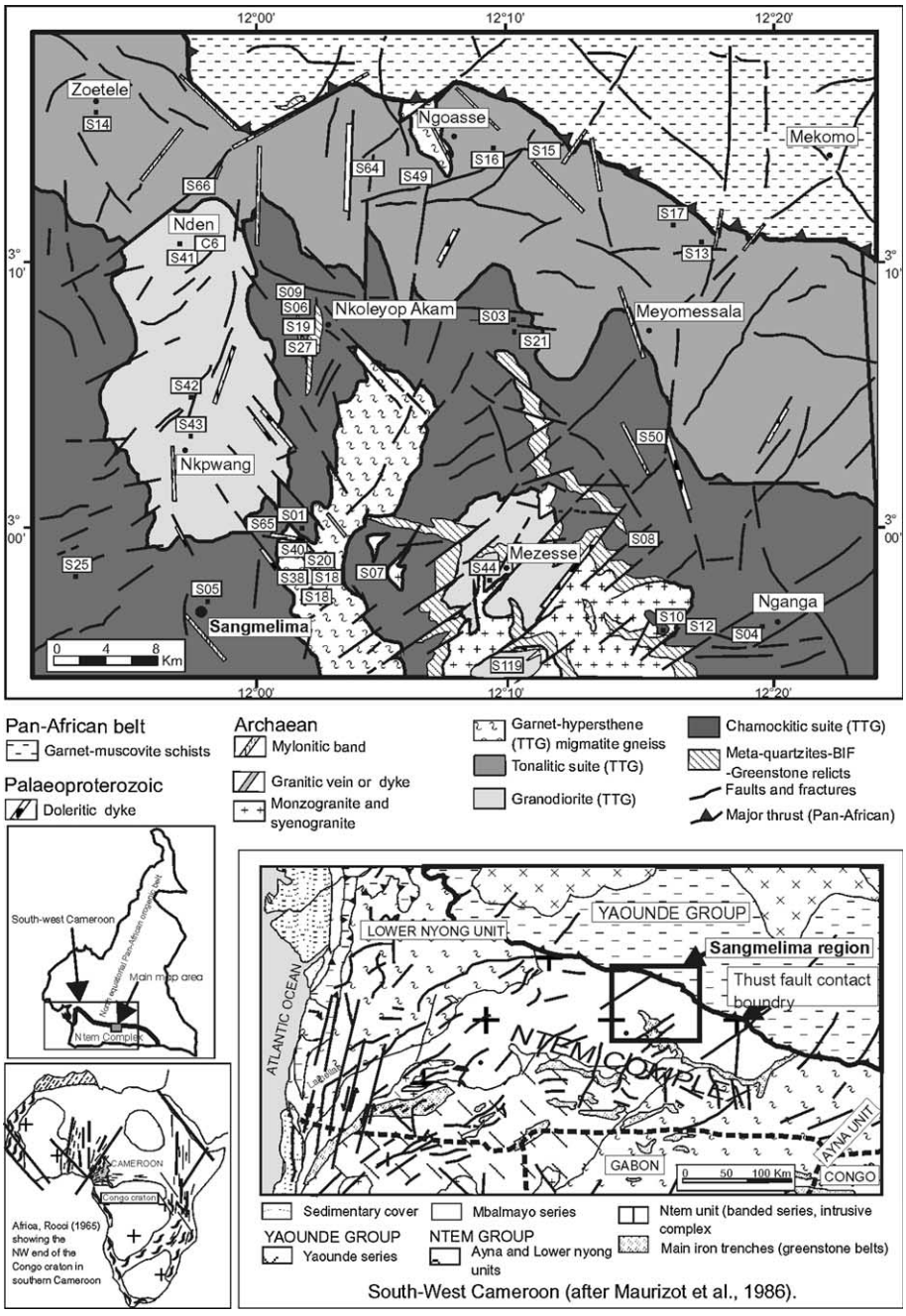

Fig. 1. Regional geological map of the north-western part of the Congo craton (Ntem complex) and thrust contact with the North Equatorial Pan-African orogenic belt in South Cameroon. Main map shows the geology of the Sangmelima region and the distribution of TTG suite.

3. Petrography

Charnockitic TTG form a suite that ranges in modal composition from fine-medium grained norites to medium–coarse grained more felsic enderbites, charnoenderbites and charnockites. The rock suite often occurs in massifs with diffuse or penetrative contacts that portray heterogeneities due probably to magmatic differentiation. This rock suite often shows ''migmatisation'', i.e. imprints of partial melting characterized by light quartzofeldspathic or granitic melts in association with melanocratic restitic schlieren that confer a banded structure to the rock. Norites and monzonorites sometimes occur as small individual massifs or as centimetric xenoliths in various massifs, thereby contributing to the primary structure of these rocks. They may also occur as brecciated or fusiform enclaves (20–40 cm long) in less mafic members. Enderbites and charnoenderbites form metric and decametric xenoliths in slightly oriented granites. Charnockitic suite outcrops are generally

crosscut by veined rocks (aplites and pegmatites) and granitic dykes as well as by mylonitic corridors.

Charnockites, charnoenderbites and enderbites are characteristically dark grey to dark brown with bluish quartz lustre (as a result of inclusions) and malgashitic feldspars. The oriented minerals define foliation and the concentration of mafic and felsic minerals define alternating mesocratic and leucocratic banding accentuated in rocks affected by partial melting. Minerals vary between 0.1 and 0.5 mm and attain 2–4 mm in coarse facies, defining granular texture with nematogranoblastic or granoclastic tendencies in oriented samples near shear corridors. In this deformed facies, a second generation of recrystallized interstitial plagioclase microblasts rim the primary porphyroblastic phases. Norites commonly display cumulate textures. Two mineral parageneses are identified in these rocks. The main mineral phases of the first generation consist of subautomorphic hypersthene and clinopyroxene, reddish-brown biotite, brown hornblende, antiperthitic An_{17-32} plagioclase and interstitial quartz. Main accessories include zircon, apatite, ilmenite and magnetite. The second paragenesis is composed of green hornblende-actinolite and scarce biotite in coronitic positions around pyroxenes, biotite-leucoxene on opaque oxides, and epidote and sericite after feldspars.

The tonalites show a medium to coarse grained (0.2–3 mm) texture, commonly spotted with bluish quartz. Penetrative or diffuse contacts are common between the three facies of the tonalitic suite; a leucocratic and coarse grained facies of trondhjemitic composition, a mesocratic-melanocratic and medium grained facies of dioritic composition and a meso-leucocratic medium grained facies of tonalitic composition. Nodule-like dioritic facies with cumulate texture represent an early crystallized member of the tonalitic suite. Amphibole preferentially defines localised magmatic foliation. In deformed rocks, the texture becomes heterogranoblastic with nested quartz and develops protomylonitic features characterized by polygonised quartz near shear zones. The rock is generally heterogranular with xenomorphic to subautomorphic plagioclase and interstitial quartz. Essential minerals of this rock group include subhedral plagioclase (commonly An_{16-22}, with An_{27-28} in dioritic cumulates and albite (An_{7-10}) in trondhjemitic facies), microcline and quartz in association with accessory zircon, apatite, ilmenite and magnetite. Ferromagnesian minerals are biotite, minor brown and green hornblende with altered clinopyroxene in mesocratic and melanocratic facies. Coronitic association of reddish brown biotite, opaque oxides and quartz around brown hornblende phenocrysts is observed in the dioritic facies.

The granitic suite includes granodiorites and monzogranites. They are characterized by the conspicuous absence of hypersthene as compared to the members of the charnockitic suite. Granodiorites represent the main rock type. They are dark grey and medium to coarse grained. Biotite is the major mafic phase. It is a high titanium reddish-brown biotite, sometimes in symplectitic association with quartz and opaque minerals. Minor clinopyroxene and brown hornblende blebs coexist with green hornblende and oxides. Plagioclase (An_{12-17}) occurs as subhedral to anhedral poikilitic laths. Microcline is the principal K-feldspar; it is often perthitic and poikilitic. Accessories include zircon, apatite and opaque minerals, with chlorite and epidote as secondary phases. Monzogranites are slightly coarser and pinkish grey. The contacts with the granodiorites are always diffuse or progressive. However, a pegmatitic variety of this rock type often forms veins in the granodiorite. Microcline is the characteristic feldspar in this rock and is commonly phenocrystic while plagioclase is less abundant and albitic (An_{3-7}). Myrmekites often occur at the contact between the two feldspars. Quartz is a major phase. Red–brown biotite is the principal ferromagnesian mineral but more or less altered clinopyroxene and green hornblende are locally present. Accessories include zircon, apatite and opaque minerals.

4. Analytical techniques

Major and trace elements (Ba, Cr, Nb, Ni, Rb, Sr, V, Y, Zn, Zr) were analysed by X-ray fluorescence (XRF) on fused powder discs at the University of Tuebingen, using methods similar to those described in Norrish and Hutton (1969). Loss on ignition (LOI) was determined after igniting 1 g of rock sample powder in quartz crucibles at 1000 °C for 1 h. Analytical uncertainties are estimated at less than 1% for major elements and between 2% and 5% for trace elements. Other trace elements (Hf, Ta, W, Pb,Th, U) and REE were analysed by inductively coupled plasma mass spectrometry (ICP-MS) in the laboratory of the Museum of Central Africa, Belgium. Analytical uncertainties for REEs are estimated at less than 10%.

For Sr and Nd isotope analyses, about 50 mg of whole-rock sample powder was spiked with mixed ^{84}Sr–^{87}Rb and ^{150}Nd–^{149}Sm tracers prior to dissolution in HF acid at 180 °C and under high pressure in polytetrafluor-ethylene (PTFE) reaction bombs. Element separation (Rb, Sr and REE) was performed in quartz columns containing a 5 ml resin bed of AG 50W-X12, 200–400 mesh, conditioned and equilibrated with 2.5 N HCl. For Sm and Nd separation, 1.7 ml Teflon powder coated with HDEHP (Di-Ethyl Hexyl Phosphate) as cation exchange medium was employed in smaller quartz columns, equilibrated with 0.18 N HCl. For mass spectrometric analyses, Sr was loaded with a Ta-HF activator and measured on a single W filament. Rb was loaded as a chloride and Sm and Nd were loaded as phosphates and measured in a double Re-filament

configuration mode. All analyses were performed using a Finnigan MAT 262 thermal ionisation mass spectrometer (TIMS) equipped with 8 Faraday cups in a static collection mode. The $^{87}Sr/^{86}Sr$ ratios were normalized to $^{86}Sr/^{88}Sr = 0.1194$, the $^{143}Nd/^{144}Nd$ ratios to $^{146}Nd/^{144}Nd = 0.7219$, and Sm isotopic ratios to $^{147}Sm/^{152}Sm = 0.56081$. Analyses of 24 separate loads of Ames metal (Geological Survey of Canada, Roddick et al., 1992), during the course of this study (01–09/2000), gave a $^{143}Nd/^{144}Nd$ ratio of 0.512125 ± 10 ($\pm 2\sigma$ error of the mean) and within the same period, the NBS 987 Sr standard yielded $^{87}Sr/^{86}Sr$ ratio of 0.710259 ± 12 ($n = 28$). Total procedural blanks (chemistry and loading), were <200 pg for Sr and <100 pg for Nd. Least-square regression of the Rb–Sr and Sm–Nd isotopic data with assessment of fit using the mean square of the weighted deviates (MSWD), were calculated after Brooks et al. (1968) and Wendt (1986). All regression errors are quoted at the 2σ level. Nd-model ages and ε_{Nd} were calculated using present day CHUR values of 0.1967 for $^{147}Sm/^{144}Nd$ (Jacobson and Wasserburg, 1980) and 0.512638 for $^{143}Nd/^{144}Nd$ (Goldstein et al., 1984). Model ages were determined using depleted mantle values as given in Liew and Hofmann (1988). Decay constant for ^{87}Rb (1.42×10^{-11} a^{-1}) was taken from Steiger and Jäger (1977) and for ^{147}Sm (6.54×10^{-12} a^{-1}) from Lugmair and Marti (1978).

5. Results

5.1. Major elements

Charnockitic and tonalitic suite members are characterized by a wide SiO_2 variation (54–70% for charnockitic TTG and 58–76% for tonalitic TTG), qualifying them as intermediate and felsic rocks. The variation in SiO_2 concentration for granodiorites (65–76%) indicates their felsic composition. With the exception of Na_2O in the tonalitic suite, all major elements for the three rock types shown in Fig. 2 tend to decrease with increasing SiO_2. A large variation of Al_2O_3 concentration (14–18%) is shown by the charnockitic suite in the 54–60% silica range.

Although the ASI index (A/CNK = [Al_2O_3/($CaO + Na_2O + K_2O$) mol%]) indicates metaluminous and peraluminous composition for the three TTG rock groups, a dominant metaluminous character ($0.56 < (A/CNK) < 0.99$) is observed for members of the charnockitic suite while a greater proportion of tonalites and granodiorites show peraluminous character (A/CNK > 1, Table 1). However, ASI values $\leqslant 1.1$ point to an I-type character (e.g. White and Chappell, 1977) for these granitoids (Fig. 3a).

The charnockitic suite is characterized by a lower total alkali content ($3\,wt\% < Na_2O + K_2O < 6\,wt\%$) as compared to the tonalitic ($5\,wt\% < Na_2O + K_2O < 7\,wt\%$) and the granodioritic ($6\,wt\% < Na_2O + K_2O < 7\,wt\%$) suites. High Na_2O/K_2O ratios (2.2–9.4, but 1.7 in S06) are observed in charnockites and tonalites (2.2–6.7), while lower ratios (0.9–1.7, but 3.0 in S21) mark the granodiorites. Hence low and medium-K compositions (Fig. 3b) characterize charnockites and tonalites and medium to high-K compositions mark granodiorites (cf. criteria of Gill, 1981; Le Maitre et al., 1989). The sum of $Na_2O + K_2O$ does not increase with increasing silica in the three rock suites. In the normative diagram An–Ab–Or (Fig. 4a) used for rocks with >10% normative quartz, tonalites and charnockites plot in and around the average Ntem TTG field as defined by Nédélec et al. (1990). In the K–Na–Ca diagram (Fig. 4b), the granodioritic suite portrays a potassic calc-alkaline trend while the tonalites and charnockites define a sodic calc-alkaline trend (trondhjemitic trend) that is typical of Archaean TTG suites worldwide.

Ferromagnesian oxides content ($Fe_2O_{3Total} + MgO + TiO_2$) varies from 10% to 18% in the charnockitic suite, 7% to 11% in the tonalitic suite, whereas the lowest content (1% to 7%) mark the granodiorites. Ferromagnesian oxides content in tonalites and granodiorites is similar to that recorded in average adakites, i.e. ~7 wt% (Martin, 1999). $Mg\# = [Mg^{2+}/(Mg^{2+} + Fe_{Total}) \times 100$, with Fe_{Total} as $Fe^{2+}]$ varies from 60 to 32 for the charnockites and 60 to 35 for tonalites, with a general decrease with increasing SiO_2 except for two tonalite samples (S33, S38), displaying high Mg# at high-SiO_2 content. Mg# in granodiorites varies from 47 to 35.

5.2. Trace elements

There is a constant decrease of Ni, Cr, Zn and V contents with increasing silica abundance (Table 1). The average Ni content in charnockites and tonalites and some granodiorite samples is similar to the average Ni content of ~24 ppm in adakites (Martin, 1999). Granodiorites are richer in Ba and Rb and poorer in Cr, Nb, V and Zn than tonalites and charnockites. Zr and Sr show a similar average abundance in all the rock types while generally low concentrations are observed for Y and Ti in all the rock types. K/Rb ratios vary between 144 and 942 in all the rock types with an average of about 420 for the charnockites, 393 for the tonalites and 400 for granodiorites. These values are higher than those reported in TTGs from many cratons (e.g. 200–300 after Condie, 1981). However, such high values are known in some Archaean cratons e.g. Jahn and Zhang (1984) for the Sino-Korean craton, Sheraton and Black (1983) and Sheraton and Collerson (1984) for the Antarctic craton. Rb/Sr ratios are quite low (0.01–0.78 for charnockites, except for sample S40 with a high ratio of 1.66 due to a particularly low Sr content of 56 ppm,

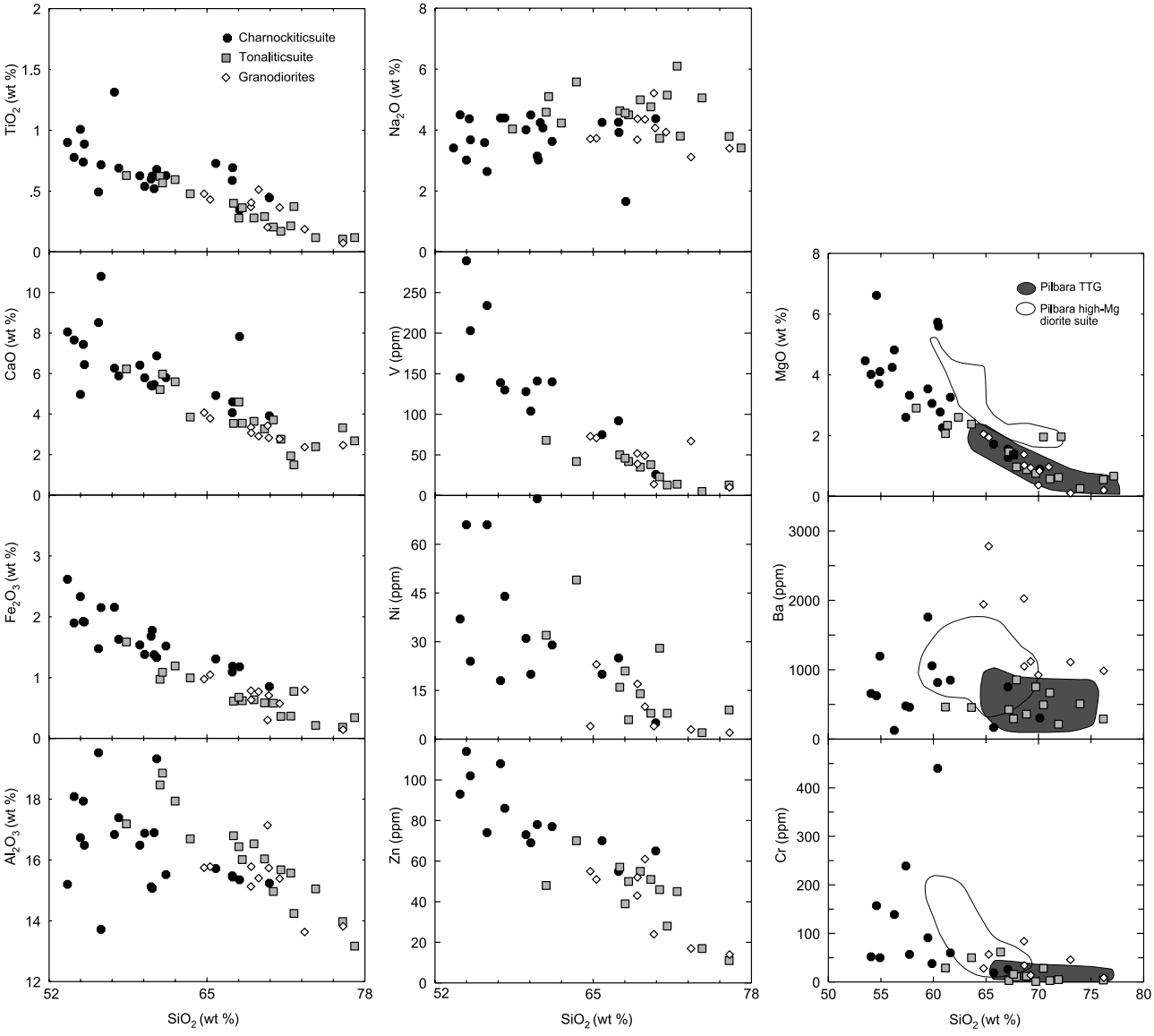

Fig. 2. Harker diagrams for selected major and trace elements. Filled circles represent the charnockitic suite, filled squares represent tonalitic suite, filled diamonds symbolize granodiorites.

0.02–0.34 for the tonalites and 0.03–0.27 for granodiorites). Sr/Y ratio versus Y diagram (Fig. 5) shows that the composition of Sangmelima TTG are similar to TTGs derived by partial melting of eclogitic facies Archaean mafic rocks represented by model curve 1 in that diagram (e.g. Drummond and Defant, 1990).

Primordial mantle-normalized diagrams (Fig. 6a) show generally similar patterns for the three Sangmelima TTG rock types, with negative Nb, Ta anomalies and positive Ba, La anomalies. Positive and negative Th anomalies occur in all the three TTG rock types. Lowest average abundances for Pb (7.2 ppm), Th (3.7 ppm) and U (0.5 ppm) mark the charnockites while the highest amounts (Pb = 14.9 ppm, Th = 9.2 ppm and U = 0.8 ppm) occur in granodiorites. These values give Th/U ratios of 0.5–9.6 for charnockites. A similar range of 0.5–9.2 characterizes the tonalites except for the leucocratic vein sample S18, with a very high ratio of 20.9, while granodiorites yield a wider range from 0.4 to 16.1.

Chondrite normalized REE patterns are presented in Fig. 6b. Charnockites are generally enriched in LREE with respect to HREE, with La_N/Yb_N ratios ranging from 11 to 28 but the quartz-norite sample S10 displays an almost flat pattern with $La_N/Yb_N = 2.1$. Except for the sample S04, an enderbite with a strong positive Eu anomaly (Eu/Eu* = 1.81), all the other samples portray slight negative Eu anomalies with Eu/Eu* between 0.83–0.92. The sample S04 shows the lowest REE abundance and the most depleted HREE pattern.

Table 1
Major and trace element concentrations for Sangmelima TTG suite: charnockitic suite

Sample	S07	S40	S06	S10	S03	S01	S05	S08	S09	S04	S25	S12
SiO_2	54.1	54.6	54.9	56.3	57.4	59.5	59.9	60.4	61.6	65.7	67.1	70.1
TiO_2	0.8	1.0	0.89	0.72	1.3	0.63	0.54	0.60	0.63	0.73	0.59	0.45
Al_2O_3	18.1	16.7	16.5	13.7	16.8	16.5	16.9	15.1	15.5	15.7	15.5	15.2
Fe_2O_3	8.6	10.6	8.7	9.8	9.8	7.0	6.3	7.6	6.9	5.9	5.0	3.9
MnO	0.12	0.2	0.12	0.12	0.12	0.11	0.09	0.13	0.10	0.08	0.05	0.05
MgO	4.0	6.6	4.1	4.8	2.6	3.5	3.1	5.7	3.3	1.7	1.6	0.10
CaO	7.7	5.0	6.4	10.8	6.3	6.4	5.8	5.4	5.8	4.9	4.1	3.9
Na_2O	4.5	3.0	3.7	2.6	4.4	4.0	4.5	3.2	3.6	4.3	4.3	4.4
K_2O	1.2	1.6	2.2	0.52	0.93	1.8	1.7	1.3	1.7	0.45	1.2	0.92
P_2O_5	0.3	0.11	0.42	0.10	0.25	0.26	0.22	0.21	0.24	0.12	0.16	0.14
LOI	0.41	0.6	0.72	0.16	0.10	0.41	0.57	0.40	0.16	0.18	0.34	0.31
Total	99.9	100.2	98.9	99.8	100.2	100.4	99.7	100.3	99.7	100.0	99.9	100.4
$Na_2O + K_2O$	5.7	4.6	5.9	3.2	5.3	5.8	6.2	4.4	5.3	4.7	5.5	5.2
Na_2O/K_2O	3.8	1.9	1.7	5.1	4.7	2.2	2.6	2.5	2.2	9.4	3.5	4.7
Ab/An	1.5	1.1	1.4	0.9	1.2	1.6	1.8	1.1	1.4	1.6	1.8	1.9
A/CNK	0.8	1.1	0.82	0.56	0.86	0.82	0.86	0.93	0.85	0.96	0.98	0.99
Mg#	48.0	55.3	48.3	49.4	34.5	50.1	49.1	59.8	48.4	36.4	38.3	31.5
Ba	659	626	1197	129	479	1760	1058	818	850	169	753	305
Cr	52	157	50	139	239	91	38	440	60	19	26	0
Nb	4	6	6	15	7	2	2	4	2	3	6	6
Ni	37	66	24	66	18	31	20	74	29	20	25	5
Rb	23	93	77	9	14	31	34	38	60	4	28	21
Sr	460	56	647	351	452	627	628	415	630	424	374	269
V	145	289	203	234	139	128	104	141	140	75	92	26
Y	16	28	21	16	22	14	14	15	12	7	8	10
Zn	93	114	102	74	108	73	69	78	77	70	55	65
Zr	130	79	179	48	196	143	169	118	152	170	180	342
K	9819	13,479	18,111	4283	7736	15,073	14,309	10,383	13,761	3768	10,093	7669
La			39.0	5.2	31.9			16.8		7.4	25.1	
Ce			80.7	13.5	63.6			35.6		14.4	45.1	
Pr			9.8	1.6	7.5			4.2		1.5	4.8	
Nd			38.3	7.2	29.4			16.9		5.9	16.7	
Sm			6.9	2.2	6.2			3.3		1.2	3.0	
Eu			1.7	0.68	1.8			0.95		0.70	0.73	
Gd			5.8	2.8	5.6			3.0		1.1	2.4	
Dy			4.0	2.8	4.3			2.4		1.0	1.5	
Ho			0.76	0.6	0.87			0.45		0.15	0.28	
Er			2.1	1.8	2.2			1.3		0.44	0.76	
Yb			1.9	1.7	1.7			1.1		0.41	0.60	
Lu			0.24	0.23	0.22			0.16		0.06	0.07	
Hf			4.8	1.3	5.3			2.6		3.8	3.8	
Ta			0.14	0.05	0.21			0.15		0.12	0.12	
W			0.80	–	0.89			1.00		0.64	0.60	
Pb			12.3	6.4	6.9			5.1		3.9	9.1	
Th			8.1	1.2	7.0			0.36		0.05	5.9	
U			0.99	0.30	1.1			0.31		0.08	0.62	
ΣREE			191.1	40.3	155.2			86.0		34.4	100.9	
K/Rb	427	145	235	476	553	486	421	273	229	942	261	365
Rb/Sr	0.05	1.66	0.12	0.03	0.03	0.05	0.05	0.09	0.10	0.01	0.08	0.78
Th/U			8.2	4.1	6.5			1.2		0.6	9.6	
La_N/Yb_N			14.1	02.1	12.4			10.5		12.1	28.3	
Eu/Eu*			0.83	0.84	0.92			0.93		1.81	0.84	

Major and trace element concentrations for Sangmelima TTG suite: tonalitic suite

Sample	S49	S15	S14	S13	S50	S64	S18	S20	S33	S17	S66	S16	S38
SiO2	57.7	61.1	63.6	67.2	67.6	67.9	68.9	69.8	70.5	71.9	71.1	74.0	76.2
TiO2	0.69	0.62	0.48	0.40	0.28	0.36	0.28	0.29	0.21	0.21	0.17	0.12	0.11
Al_2O_3	17.4	18.5	16.7	16.8	16.4	16.0	16.5	16.0	15.0	15.6	15.7	15.1	14.0
Fe_2O_3	7.4	4.4	4.5	2.8	3.1	2.8	2.9	2.7	2.6	1.7	1.6	0.97	0.84

(*continued on next page*)

Table 1 (*continued*)

Sample	S49	S15	S14	S13	S50	S64	S18	S20	S33	S17	S66	S16	S38
MnO	0.22	0.06	0.08	0.03	0.04	0.04	0.04	0.04	0.05	0.02	0.02	0.02	0.01
MgO	3.3	2.1	2.4	1.5	1.4	0.97	0.88	0.76	2.0	0.63	0.57	0.26	0.55
CaO	5.9	5.2	3.9	3.5	4.6	3.6	3.6	3.3	3.7	1.9	2.8	2.4	3.3
Na_2O	4.4	4.6	5.6	4.6	4.6	4.5	4.5	4.8	3.7	6.1	5.2	5.1	3.8
K_2O	1.4	1.6	1.1	1.5	0.69	1.9	1.2	1.7	1.2	1.1	1.4	1.4	1.01
P_2O_5	0.15	0.22	0.16	0.10	0.07	0.12	0.09	0.05	0.03	0.09	0.08	0.01	0.05
LOI	0.69	1.8	1.3	1.5	0.76	1.1	0.48	0.53	0.60	0.94	0.74	0.57	0.42
Total	99.4	100.3	100.0	100.1	99.6	99.4	100.0	99.9	99.6	100.2	99.5	99.9	100.3
$Na_2O + K_2O$	5.8	6.2	6.7	6.1	5.3	6.4	6.1	6.4	4.9	7.2	6.6	6.5	4.8
Na_2O/K_2O	3.2	2.9	4.9	3.1	6.7	2.4	4.4	2.9	3.1	5.6	3.7	3.6	3.8
Ab/An	1.6	1.6	2.7	2.3	1.7	2.2	2.4	2.5	1.7	5.6	3.2	3.5	1.9
A/CNK	0.90	0.99	0.96	1.1	0.99	1.01	1.03	1.02	1.1	1.1	1.04	1.1	1.1
Mg#	47.1	48.1	51.0	51.1	46.9	40.4	37.6	36.1	59.5	42.7	40.8	34.7	56.4
Ba	462	464	458	425	294	855	360	754	496	216	669	509	291
Cr	57	29	50	3	16	11	12	1	28	5	3	–	4
Nb	10	1	3	4	–	1	4	1	1	3	1	2	3
Ni	44	32	49	16	21	6	14	8	28	–	8	2	9
Rb	67	50	22	41	9	62	11	33	23	27	38	26	17
Sr	195	329	437	714	529	411	376	372	236	285	652	416	144
V	130	68	42	50	46	42	35	38	23	14	13	5	13
Y	28	8	21	2	3	7	8	6	2	3	1	3	1
Zn	86	48	70	57	39	50	55	51	46	45	28	17	11
Zr	152	172	134	104	174	135	207	252	104	136	93	88	61
K	11,537	13,379	9412	12,417	5702	15,662	9528	1375	9977	9097	11,720	11,554	8358
La				12.0			51.1			21.2		5.9	
Ce				20.2			89.9			33.9		10.7	
Pr				1.7			8.9			3.3		0.89	
Nd				5.6			28.9			10.2		3.0	
Sm				0.87			4.0			1.4		0.42	
Eu				0.39			0.70			0.38		0.25	
Gd				0.69			2.7			0.86		0.29	
Dy				0.30			1.2			0.36		0.24	
Ho				<0.05			0.19			<0.05		<0.05	
Er				0.15			0.50			0.13		0.25	
Yb				0.10			0.51			0.13		0.33	
Lu				<0.01			0.07			<0.01		0.04	
Hf				2.2			5.3			3.1		2.2	
Ta				0.08			0.06			<0.05		<0.05	
W				0.87			1.5			0.78		0.58	
Pb				6.8			17.2			7.6		12.8	
Th				0.93			28.2			3.7		0.22	
U				0.23			1.4			0.40		0.46	
ΣREE				42.1			188.7			71.9		22.4	
K/Rb	172	268	428	303	634	253	866	417	434	337	308	444	492
Rb/Sr	0.34	0.15	0.05	0.06	0.02	0.15	0.03	0.09	0.10	0.09	0.06	0.06	0.12
Th/U				4.0			20.9			9.2		0.5	
La_N/Yb_N				82.4			68.1			114.0		11.8	
Eu/Eu*				1.6			0.65			1.04		2.2	

Major and trace element concentrations for Sangmelima TTG suite: granodiorites

Sample	S65	S42	S43	S44	S19	S41	S21	C6	S119	S27
SiO_2	64.9	65.3	68.6	68.6	68.9	69.3	70.0	70.1	71.0	73.0
TiO_2	0.48	0.43	0.37	0.41	0.28	0.51	0.20	0.45	0.37	0.19
Al_2O_3	15.8	15.8	15.1	15.8	16.5	15.4	17.1	15.7	15.4	13.6
Fe_2O_3	4.4	4.8	3.6	2.9	2.9	3.5	1.4	3.2	2.6	3.6
MnO	0.06	0.06	0.05	0.04	0.04	0.03	0.03	0.03	0.03	0.03
MgO	2.1	1.9	1.4	1.02	0.88	0.94	0.37	0.84	0.97	0.11
CaO	4.1	3.8	3.3	3.0	3.6	2.9	3.4	2.8	2.8	2.4
Na_2O	3.7	3.7	3.7	4.4	5.0	4.4	5.2	4.1	3.9	3.1
K_2O	3.1	3.7	2.9	2.6	1.2	2.5	1.7	2.6	2.5	3.3
P_2O_5	0.19	0.20	0.13	0.15	0.09	0.18	0.03	0.13	0.11	0.04
LOI	0.42	0.68	0.48	0.52	0.48	0.36	0.37	–	–	0.52
Total	99.3	100.7	100.0	99.7	100.0	100.2	100.0	100.0	99.7	100.2

Table 1 (*continued*)

Sample	S65	S42	S43	S44	S19	S41	S21	C6	S119	S27
$Na_2O + K_2O$	6.8	7.4	6.6	7.0	6.1	7.0	6.9	6.6	6.5	6.4
Na_2O/K_2O	1.2	1.0	1.3	1.7	1.2	1.7	3.0	1.6	1.6	0.94
Ab/An	1.8	2.0	1.9	2.5	2.3	2.6	2.5	2.6	2.5	2.2
A/CNK	0.94	0.93	0.99	1.01	1.06	1.02	1.03	1.08	1.08	1.05
Mg#	47.9	44.7	43.4	41.3	37.9	34.9	34.9	34.1	42.5	5.51
Ba	1944	2782	2026	1051	360	1122	924			1111
Cr	28	57	84	34	12	14	0			46
Nb	2	2	3	3	1	5	2			0
Ni	4	23	0	17	14	10	4			3
Rb	81	77	48	97	11	81	21			55
Sr	524	582	528	347	376	334	549			379
V	73	71	52	39	35	49	14			67
Y	10	11	4	10	8	6	1			12
Zn	55	51	43	52	55	61	24			17
Zr	133	171	154	183	207	307	104			367
K	25,779	30,270	24,203	21,547	22,468	20,767	14,301			27,407
La		21.4	17.8	45.5		67.3	10.8			
Ce		42.6	30.0	77.8		113.0	17.2			
Pr		4.9	3.0	7.6		11.3	1.5			
Nd		17.5	10.0	24.1		33.7	4.6			
Sm		2.9	1.3	3.5		4.3	0.38			
Eu		0.77	0.61	0.59		0.91	0.48			
Gd		2.5	1.1	2.6		2.9	0.26			
Dy		1.6	0.81	1.6		1.2	0.07			
Ho		0.29	0.14	0.25		0.22	<0.05			
Er		0.82	0.40	0.65		0.54	0.02			
Yb		0.77	0.38	0.47		0.46	<0.1			
Lu		0.12	0.06	0.07		0.07	<0.01			
Hf		4.5	3.7	4.1		7.5	2.4			
Ta		<0.05	<0.05	0.60		0.15	<0.05			
W		0.66	0.58	0.51		0.99	6.5			
Pb		14.7	13.8	21.1		12.5	12.4			
Th		1.01	0.78	30.8		13.4	0.10			
U		0.39	0.60	2.3		0.83	0.24			
ΣREE		99.1	66.6	164.7		235.9	35.5			
K/Rb	318	393	504	222	330	256	681			498.3
Rb/Sr	0.15	0.13	0.09	0.28	0.17	0.24	0.04			0.15
Th/U		2.6	1.3	13.4		16.1	0.4			
La_N/Yb_N		18.8	31.3	72.9		99.7				
Eu/Eu*		0.9	1.6	0.6		0.8	4.7			

Major elements are in weight per cent while trace elements concentrations are in parts per mil (ppm); –: not determined.

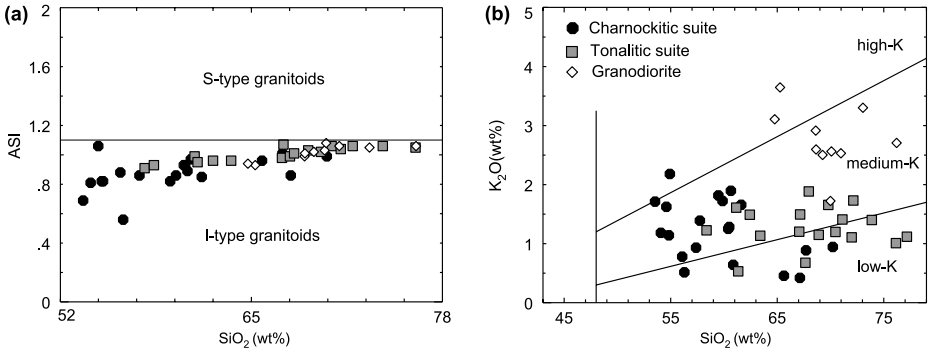

Fig. 3. (a) Aluminium saturation index (ASI) versus SiO_2 plot portraying the I-type composition for Sangmelima TTG suite. (b) K_2O versus SiO_2 diagram showing basically low and medium K composition for members of the tonalitic and chanockitic suites and medium to high K-composition for granodiorites.

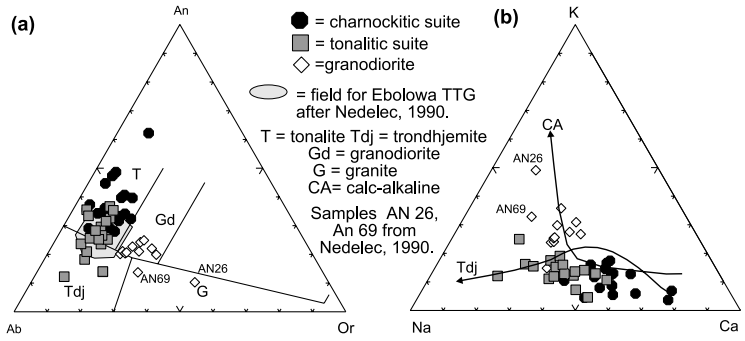

Fig. 4. (a) Normative feldspar classification from O'Connor (1965) showing the field of Sangmelima TTG in comparison with TTG from the Ebolowa area (Nédélec, 1990) of the Ntem complex. (b) Na–K–Ca diagram after Barker and Arth (1976), portraying a trondhjemitic trend for Sangmelima tonalitic and charnockitic suites and a slightly potassic calc-alkaline affinity for granodiorites.

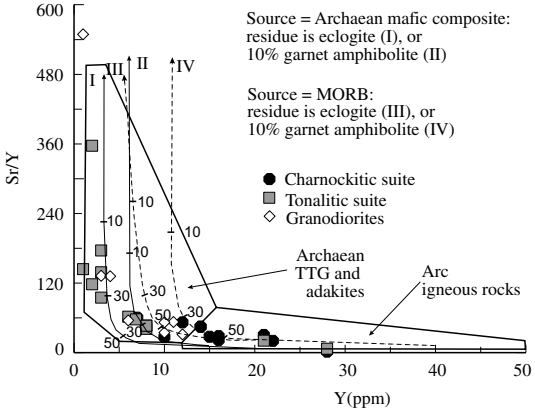

Fig. 5. Sr/Y versus Y diagram for Sangmelima TTG: samples are compatible with garnet-bearing residues. Melting curves are from Drummond and Defant (1990).

Tonalites display steeper REE pattern compared to the charnockites and granodiorites. La_N/Yb_N vary from 12 to 114. The tonalites portray high LREE fractionation ($8.1 < La_N/Sm_N < 9.3$) compared to the charnockites ($1.5 < La_N/Sm_N < 5.3$). Two of the analysed samples (S13, S16) with the lowest total REE abundance show strong positive Eu anomalies (Eu/Eu* = 1.5 and 2.1 respectively). S17 displays a slight positive Eu anomaly (Eu/Eu* = 1.04), whereas the sample S18 with the highest REE abundance displays a negative Eu anomaly (Eu/Eu* = 0.65).

Granodiorites show a stronger HREE depletion compared to charnockites with La_N/Yb_N between 19 and 100. They are more enriched in LREE (La_N/Sm_N = 4.5–18.0). However, a few granodiorite samples (e.g. S42, S43) are marked by HREE fractionation similar to that recorded in charnockites (e.g. S04, S06, S08). Three granodiorites show a negative Eu anomaly (Eu/Eu* = 0.6–0.8) while two show positive Eu anomalies (Eu/Eu* = 1.5–4.7). The REE patterns (Fig. 6b) are more or less parallel except for the sample S21 that is strongly depleted in HREE.

Based on REE characteristics, the Sangmelima TTGs could be divided into two groups. One group is marked by low REE abundance, positive Eu anomalies and strong depletion in HREE. The second group displays high REE abundance, negative Eu anomalies and enrichment in HREE. In general, the granodiorites display a stronger LREE enrichment than the charnockites and tonalites. The increase in negative Eu anomaly as well as the decrease of total REE content can be roughly correlated to the increase in SiO_2, hence to the magmatic differentiation process. All spectra (except for sample S10), are fractionated.

5.3. Sm–Nd and Rb–Sr isotopic systematics

Sm–Nd and Rb–Sr isotope compositions were determined on whole-rock samples from the three TTG rock types and data are presented in Table 2. Data for the charnockitic suite include two charnoenderbites (S03, S06), three enderbites (S04, S08, S25) and one quartznorite (S10). The spread of $^{147}Sm/^{144}Nd$ ratios is wide enough to calculate an isochron of 3049 ± 82 Ma, MSWD = 4.6 with an initial Nd value of 0.508701 ± 67. Calculations without S25 that has low ε_{Nd} values (−3.2 and −3.6, Table 2) yield an isochron of 2899 ± 93 Ma, MSWD = 2.6 (Fig. 7a) and an initial Nd value of 0.508844 ± 79. The best fit for Rb–Sr composition without S10 that has the highest initial Sr composition (Table 2), yields an isochron date of 2879 ± 55 Ma, MSWD = 4.6, with an initial $^{87}Sr/^{86}Sr$ ratio of 0.70176 ± 17 (Fig. 7a). Dates derived from the Sm–Nd isochron without S25 and from the Rb–Sr isochron without S10 are indistinguishable within error limit. Nd-model ages (T_{DM}) range from 3200 to 3010 Ma; S10 yields an older model age of 3320 Ma. T_{CHUR} ages determined for comparison with T_{DM} ages vary from 3196 to 2872 Ma. Some of these model ages

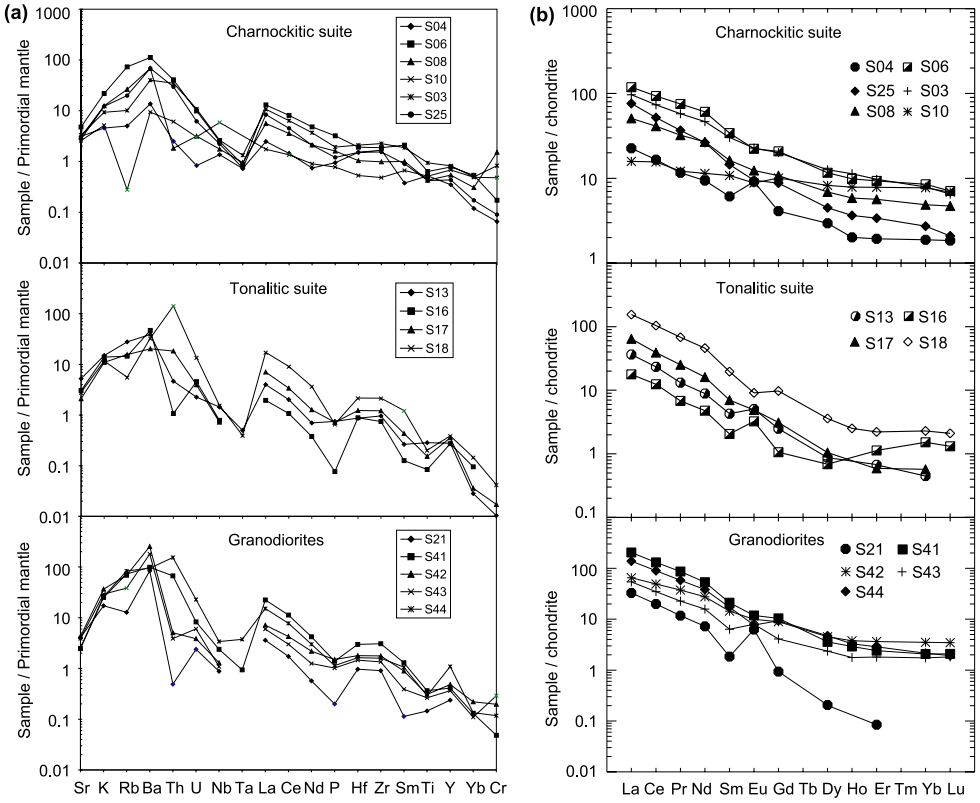

Fig. 6. (a) Primordial mantle-normalized spidergrams (to the values of Sun and McDonough, 1989). Arrangement of elements after Pearce (1983). (b) Chondrite normalized REE patterns (to the values of Boynton, 1984) for selected samples of the Sangmelima TTG suite.

Table 2
Sm, Nd, Rb and Sr abundances and isotopic whole-rock composition from Sangmelima TTG suite

	Sample	Sm	Nd	$^{147}Sm/^{144}Nd$	$^{143}Nd/^{144}Nd \pm 2\sigma_m$	$\varepsilon_{Nd2850\,Ma}$	T_{DM}/Ma	T_{CHUR}/Ma	Rb/ppm	Sr/ppm	$^{87}Rb/^{86}Sr$	$^{87}Sr/^{86}Sr \pm 2\sigma_m$	$Sr_{2850\,Ma}$
Charnockitic suite	S03	6.153	29.78	0.1249	0.511277 (9)	−0.2	3020	2876	12.17	454.2	0.0775	0.704520 (9)	0.70132
	S04	1.284	6.27	0.1238	0.511258 (7)	−0.2	3010	2872	1.407	401.2	0.0101	0.702373 (13)	0.70195
	S06	6.820	36.85	0.1118	0.510955 (9)	−1.7	3100	3009	80.9	647.9	0.3617	0.716648 (10)	0.70171
	S08	3.557	18.34	0.1172	0.511051 (8)	−1.8	3120	3027	35.15	406.2	0.2505	0.712124 (7)	0.70178
	S10	2.047	7.15	0.1731	0.512142 (9)	−1.0	3320	3196	4.639	350.4	0.0383	0.704234 (10)	0.70265
	S25a*	2.860	17.18	0.1006	0.510666 (10)	−3.2	3180	3109	26.34	352.5	0.2163	0.711372 (10)	0.70244
	S25b*	2.851	16.10	0.1075	0.510649 (10)	−3.6	3200	–					
Tonalitic suite	S13	0.976	6.338	0.0930	0.510670 (10)	−0.5	2990	2889	34.63	662.3	0.1513	0.707469 (10)	0.70122
	S16	0.510	3.148	0.0979	0.510621 (30)	−3.1	3160	3097	20.7	376.1	0.1593	0.707902 (10)	0.70133
	S17	1.578	10.89	0.0876	0.510472 (14)	−2.3	3090	3012	21.87	263.4	0.2404	0.711362 (9)	0.70144
	S18	4.545	35.01	0.0784	0.510334 (9)	−1.6	3040	2955	11.31	376.0	0.0870	0.706738 (10)	0.70314
Granodiorites	S21	0.509	4.558	0.0675	0.510137 (12)	−1.4	3010	2934	17.20	501.0	0.0993	0.705376 (9)	0.70127
	S41	5.727	53.10	0.0651	0.510161 (9)	−0.1	2940	2856	77.88	312.6	0.7226	0.730818 (10)	0.70098
	S42	3.282	20.35	0.0974	0.510739 (8)	−0.6	3010	2902	73.16	554.9	0.3819	0.717524 (10)	0.70175
	S43	1.764	13.16	0.0810	0.510432 (8)	−0.6	2990	2893	45.07	497.2	0.2624	0.712375 (9)	0.70154
	S44	4.302	32.17	0.0808	0.510472 (8)	0.3	2940	2834	94.29	325.1	0.8417	0.736627 (12)	0.70187

* Replicate analyses; $_m$error of measured value.

are identical with the isochron dates. $\varepsilon_{Nd2850\,Ma}$ values vary from −0.2 to −1.8 but much lower values of down to −3.6 are noted for S25 while initial Sr ratios range from 0.70132 to 0.70265.

The Sm–Nd and Rb–Sr system for tonalites was studied in four samples comprising three massive rocks (S13, S16, and S17) and one vein tonalite, S18 (Table 2). Sm–Nd composition of the samples does not permit

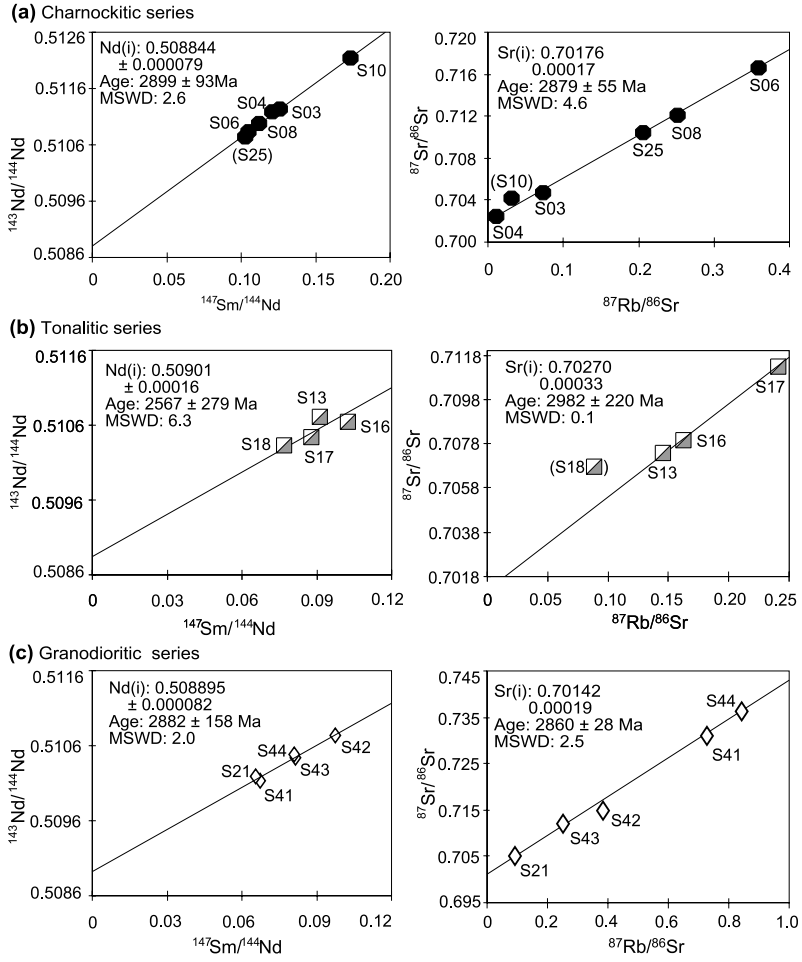

Fig. 7. Sm/Nd and Rb/Sr isochron diagrams for rocks of Sangmelima TTG suite, (a) the charnockitic suite, (b) rocks of the tonalitic suite, (c) granodiorites. Errors used for isochron calculation are 1% for $^{87}Rb/^{86}Sr$, 0.3‰ for $^{87}Sr/^{86}Sr$, 0.5% for $^{147}Sm/^{144}Nd$ and 0.03‰ for $^{143}Nd/^{144}Nd$.

a good isochron evaluation because of similar $^{147}Sm/^{144}Nd$ ratios (Fig. 7b). However, an isochron date of 2567 ± 279 Ma, MSWD = 6.3 and an initial Nd value of 0.50901 ± 16, is obtained. Except for sample S13 with an $\varepsilon_{Nd2.850}$ value of −0.5, other samples yield lower values (−2.3 to −3.1), while initial Sr ratios range from 0.70122 to 0.70314. The best fit line defined by the Rb–Sr system without the vein sample (S18), yields a date of 2982 ± 220 Ma, MSWD = 0.1 (Fig. 7b), and an initial Sr ratio of 0.70270 ± 33. Isochron dates from the two isotopic systems are identical within error. Nd-model ages (T_{DM}) for these samples vary from 3160 to 2990 Ma. T_{CHUR} ages give values between 3097 and 2889 Ma.

Granodiorite samples analysed for Sm–Nd and Rb–Sr isotope composition include the vein leucocratic sample S21 and four massif samples porphyritic S41, medium grained leucocratic S42 and coarse grained mesocratic S43 and S44 (Table 2). Their Sm and Nd isotope compositions define a best fit line with a date of 2882 ± 158 Ma, MSWD = 2.0 and Nd initial value of 0.508895 ± 82, while the Rb–Sr system gives

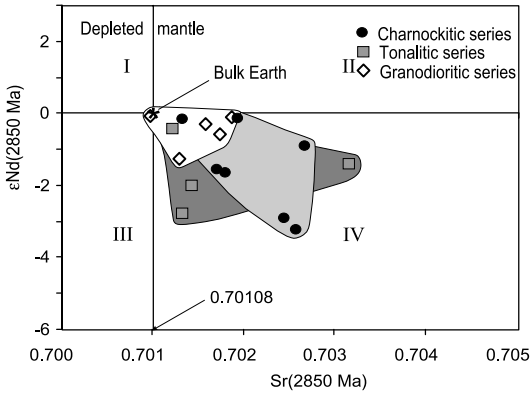

Fig. 8. $\varepsilon_{Nd(T)}$ versus $Sr_{(T)}$ correlation diagram showing the composition of Sangmelima TTG at 2850 Ma. Initial Bulk Earth composition of 0.70108 was calculated using values from DePaolo (1988) ($^{87}Rb/^{86}Sr = 0.0827$, $^{87}Sr/^{86}Sr = 0.7045$).

2860 ± 28 Ma, MSWD = 2.5 with an initial Sr ratio of 0.70142 ± 19 (Fig. 7c). Nd-model ages (T_{DM}) for granodiorite samples vary from 3010 to 2940 Ma. T_{CHUR} ages give values between 2934 and 2834 Ma. Granodiorites

Table 3
Rb and Sr isotopic composition of biotites from Sangmelima TTG

Sample	Sr (ppm)	Rb (ppm)	$^{87}Rb/^{86}Sr$	$^{87}Sr/^{86}Sr$	Bi–WR age	$^{87}Sr/^{86}Sr(i)$
Bi SO3	17.94	383.5	75.38	2.94479		
WR S03 (charno.)	454.2	12.17	0.0775	0.70452	2064 ± 20 Ma	0.70222
Bi S25	8.726	408.7	241.91	8.73361		
WR S25 (charno.)	352.5	26.34	0.2163	0.71137	2299 ± 22 Ma	0.70419
Bi S41	10.32	700.3	438.84	13.3340		
WR S41 (grano.)	312.6	78.88	0.7224	0.73082	1997 ± 19 Ma	0.71004

have relatively high $\varepsilon_{Nd2850\,Ma}$ values (0.3 to −1.4) and low initial $Sr_{2850\,Ma}$ ratios (0.70098–0.70187), compared to charnockites and tonalites. In the $\varepsilon_{Nd2850\,Ma}$ versus initial $Sr_{2850\,Ma}$ diagram (Fig. 8), all the analysed samples plot in the fourth quadrant with some close to Bulk Earth composition.

Biotite separates were also analysed for Rb–Sr composition (Table 3). Two charnockites (S03 and S25) yielded whole-rock-biotite ages of 2064 ± 20 Ma and 2299 ± 22 Ma with initial Sr ratios of 0.7022 and 0.7042, respectively. Biotite from a granodiorite (S41) gave an age of 1997 ± 19 Ma, with an initial Sr ratio of 0.7029.

6. Discussion

6.1. Major–trace elements and petrogenesis

Sangmelima region TTG are intermediate to felsic and aluminous rocks with low Yb (generally ⩽1 ppm), $Na_2O/K_2O > 1$, and high Sr and Ba values, similar to worldwide TTG complexes (e.g. Barker and Arth, 1976; Barker, 1979), that are considered to be the result of partial melting of garnet amphibolite or eclogite facies basaltic crust (e.g. Arth and Hanson, 1975; Barker and Arth, 1976; Barker, 1979; Tarney et al., 1976; Martin, 1986; Drummond and Defant, 1990; Rapp et al., 1991; Rapp, 1997). In fact, the Y versus Sr/Y correlation diagram (Fig. 5) follows the trajectory of model curve I, clearly portraying an Archaean mafic crustal source. However, a direct melting of an eclogitic subducting oceanic crust (MORB) might not be completely ruled out.

The group of samples in the three TTG rock types with low REE abundances, positive Eu anomalies and depletion in HREE, could represent cumulative feldspar rich fractions, while the other group of samples with high REE abundances, negative Eu anomalies and enriched HREE patterns, probably represent members of the various rock suites with more ferromagnesian phases and REE bearing accessories. The former probably also represent the more fractionated part of melts or low degree partial melts as indicated by high silica content. Higher HREE abundance (unusual positive HREE slope), observed in the tonalite sample S16 compared with low HREE abundance in the other two samples S13 and S17 with positive Eu anomalies (Fig. 6b), could be due to selective contamination by a garnet rich pole in the source or could represent a quenched liquid rich in HREE or it could probably represent the effect of hydrothermal alteration. Thin section observation actually shows some degree of alteration in S16 which however, is not different from that in the other samples. In general, tonalites and granodiorites that are more felsic than members of the charnockitic suite display LREE enrichment and this could be explained by the fact that LREEs are incompatible during fractional crystallization of tonalitic/granodioritic melts. The low concentration of Y and Ti and high La_N/Yb_N ratios reflected in the relatively steeper REE patterns (Fig. 6b), could be due to a melting residue containing garnet, titanite and or ilmenite. In fact, highly fractionated REE compositions have been reported from many areas (e.g. the central Andean rocks) and interpreted as a result of residual garnet in the sources (e.g. Kay et al., 1994; Mpodozis et al., 1995; Kay and Abbruzzi, 1996). Similar observations were made in magmatic rocks from the Variscan Odenwald, Germany (Altherr et al., 1999). Experimental studies (e.g. Irving and Frey, 1978; Green and Pearson, 1985) have shown that garnet has high mineral/melt partition coefficients for the HREE and it is therefore considered as the key mineral to produce high La_N/Yb_N ratios in Sangmelima TTG. These REE characteristics suggest that the Sangmelima TTG magmas could have been formed within the stability field of garnet from a subducted eclogitic crust. Another possibility to get a garnet signature would be by melting a thickened crust of about 40 km (e.g. Holdaway, 1971; Kay and Kay, 1991; Spear, 1993).

Average Th/U ratios of the TTGs (5 for charnockites, 4.6 for tonalites, without considering the value of 20.9 from sample S18 and 6.7 for granodiorites) are higher than the estimated Bulk Earth value of 3.85 and the value of 3.9 ± 0.1 deduced from igneous rocks of various ages (e.g. Galer and O'Nions, 1985), and more than double the upper mantle value (⩽2.5, e.g. Jochum et al., 1983). In granulite fields such high ratios could be explained by the differential loss of these elements during metamorphism. But such high Th/U ratios like high

K/Rb ratios in the case of the Sangmelima rocks which do not show granulite facies mineral assemblages, are probably due to originally low U and Rb sources for these rocks (e.g. Nédélec et al., 1990; Tchameni, 1997; Shang, 2001). However, the poor correlation between Rb and Sr and considerable variation in Th/U ratios may actually point to some degree of alteration.

The Mg#–SiO_2 plot (Fig. 9a) shows a complex setting for Sangmelima TTG. In fact, the idea in this diagram as presented by Smithies (2000) and Smithies and Champion (2000), comparing high-Mg# rocks and adakites (TTG chemical equivalents, e.g. Defant and Drummond, 1990), is that younger TTG magmas (<3.0 Ga) ascending through the mantle were contaminated by it, hence displaying high Mg# and low SiO_2 content. Smithies (2000) noted that typical mid-ocean ridge basalt has an Mg# of around 60 such that partial melting (~20%, e.g. Rapp et al., 1999) required to generate an adakitic magma should yield Mg# considerably lower than 60 (e.g. Mg#~45, Rapp, 1997). Therefore, adakitic rocks with Mg# $\gtrsim$50 must have reacted with material significantly more mafic than basalt and contamination by mantle peridotite was suggested (e.g. Yogodzinski et al., 1995; Rapp et al., 1999). This interpretation would have important geodynamic implications. By comparison, tonalites in this study show both high Mg# versus low SiO_2 and high Mg# versus high-SiO_2 content, and plot in the field of younger TTG of Smithies (2000) (Fig. 9b). Most charnockite samples (Fig. 9b) show high-Mg#–low SiO_2 contents with thus a greater overlap in the adakite and high-Mg diorite suite fields (Fig. 9a), thereby suggesting greater mantle wedge material contamination with inference for a subduction setting similar to that of Cenozoic adakites. The higher Mg# versus higher SiO_2 content for some tonalites is similar to the composition of high Al type TTG of the Southern Superior Province of Canada, thought to have interacted with the mantle wedge (e.g. Feng and Kerrich, 1992). Granodiorites show moderate-low-Mg# and high SiO_2 content, but plot like tonalites in the younger TTG field and at the upper limit of the older TTG field (Fig. 9b) of Smithies (2000). We interpret these low Mg# versus high SiO_2 TTG rocks, that do show enough evidence of mantle material contamination to be the more fractionated part of the TTG magma. However it is generally argued that low Mg# versus high SiO_2 rocks might not have interacted with the peridotitic mantle wedge, implying for instance their genesis in a flat subduction regime (e.g. Smithies et al., 2003), or an underplating tectonic setting that excluded the mantle wedge. Martin and Moyen (2002) also suggest that subducted slabs may have melted at a level shallow enough to have effec-

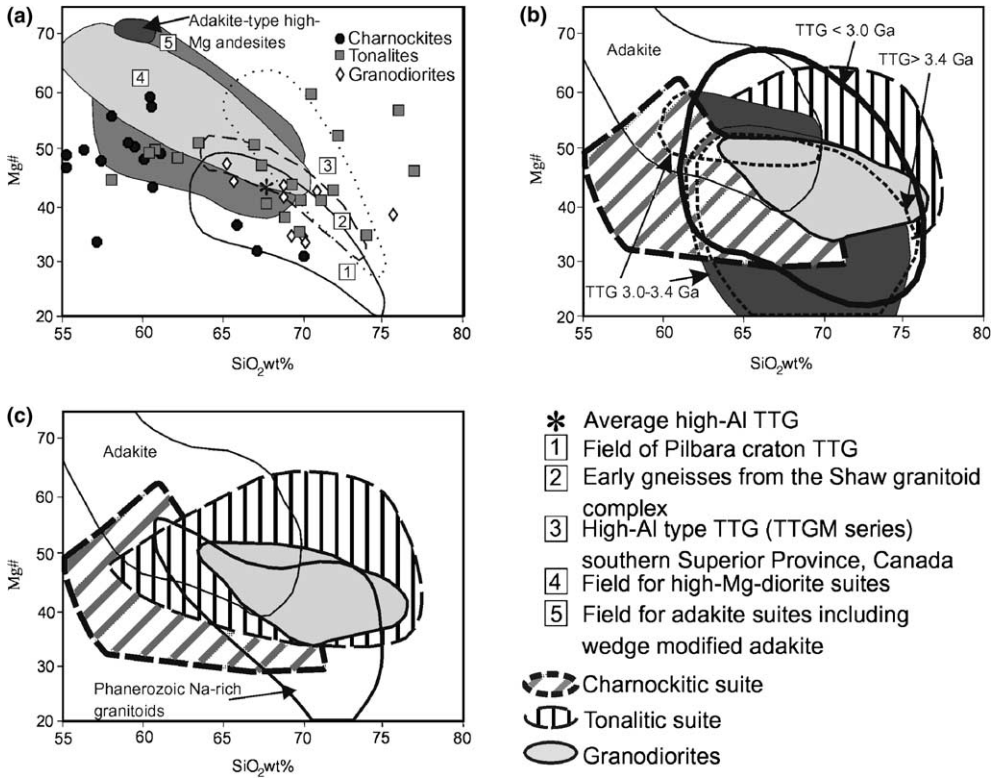

Fig. 9. Diagrams of silica versus Mg# (Mg-number), (a) comparison of Sangmelima TTG to other TTG complexes and related rocks. Fields from Smithies and Champion (2000) and references therein, (b) comparison of Sangmelima TTG and other TTGs, fields from Smithies (2000), (c) comparison of Sangmelima TTG fields and adakites and Phanerozoic Na-rich granitoids from Smithies (2000).

tively precluded any interaction between the slab-melts and the mantle. In another view, Defant and Kepezhinskas (2001) suggest that one reason why some Archaean TTG suites show little or no evidence for interaction with the mantle wedge might be that the very high volumes of melt driven off the thick slabs swamped the thin mantle wedge.

In another consideration, some Sangmelima TTG showing lower Mg#–higher SiO_2 composition appear more consistent with melting of hydrous basaltic material at the base of the Archaean crust under a typical Archaean geotherm, a case that would be similar to the Pilbara craton (e.g. Bickle et al., 1983, 1989, 1993) and that does not necessarily require a subduction setting. De Wit (1998) speculated that hydrated basaltic crust at the origin of such rock types was stacked into thrust piles in early Archaean times and underwent internal differentiation by partial melting to form Earth's earliest continental fragments.

6.2. Sm–Nd and Rb–Sr isotopic dates

The Sm–Nd and Rb–Sr chronometric systems (Fig. 7) yield similar isochron dates within error for Sangmelima TTG rock suites (2899 ± 93 Ma and 2879 ± 55 Ma for the charnockites, 2567 ± 279 Ma and 2982 ± 220 Ma for the tonalites and 2882 ± 158 Ma and 2860 ± 28 Ma for granodiorites). The above dates for the charnockites are similar to the whole-rock Rb–Sr isochron dates of 2890 ± 270 Ma and 2859 ± 65 Ma determined by Delhal and Ledent (1975) and by Lasserre and Soba (1976, 1979) respectively, on similar rock types from other parts of the Ntem complex. The charnockites yield an average Pb–Pb zircon crystallization age of 2884 ± 10 Ma (Shang, 2001), similar to an igneous crystallization age of 2896 ± 7 Ma reported by Toteu et al. (1994), using U–Pb zircon data and a more precise Pb–Pb zircon date of 2912 ± 1 Ma reported by Tchameni (1997), on a population of zircons from charnockites from some localities of the Ntem complex. Given these identical age data from the same rock types from other parts of the Ntem complex, we interpret the charnockitic isochron date from the Sangmelima region as close approximation to crystallization time. The Sm–Nd isochron date of 3049 ± 82 Ma for the charnockites calculated including sample S25 that appears to be more crustally contaminated as suggested by its low ε_{Nd} values (−3.2 and −3.6, Table 2), therefore appears to be of no geological significance. As for the tonalites, Lasserre and Soba (1976) report a Rb–Sr isochron date of 2780 ± 50 Ma from north of Ebolowa. Using the same method, Nzenti et al. (1988) presented a similar isochron date of 2790 ± 120 Ma on Soo tonalites. Sangmelima tonalites have an average Pb–Pb zircon crystallization age of 2825 ± 11 Ma (Shang, 2001) similar to a Pb–Pb zircon evaporation date of 2833 ± 1.2 Ma reported by Tchameni (1997), from tonalites of the Ebolwa area. As such, it appears difficult from our Rb–Sr and Sm–Nd data (2567 ± 279 Ma and 2982 ± 220 Ma respectively), to suggest the emplacement timing for the tonalites in the Sangmelima region. For the granodiorites, both Sm–Nd and Rb–Sr isochron systems yield identical dates within error of ~2880 Ma. This date is similar to the Rb–Sr isochron date of 2880 ± 70 Ma reported by Lasserre and Soba (1976) on Ntem granodiorites and could therefore be of geologic significance. However, the Sangmelima granodiorites have an average zircon Pb–Pb crystallization age of 2832 ± 12 Ma (Shang, 2001). It is also worth noting that a younger zircon Pb–Pb date of 2687 ± 3 Ma (Tchameni et al., 2000) has been reported for seemingly end members of the high K-granitoids suite (for which granodiorites would be earlier crystallized members), from the eastern part of the Ntem complex and 2670 ± 11 Ma (Shang, 2001) for similar rocks from the western part.

Although a slight difference is observed between some T_{DM} and T_{CHUR} ages (Table 2), they are only slightly older when compared with the isochron dates (Fig. 7), suggesting early Mesoarchaean and late Paleoarchaean time of extraction of the TTGs from their sources. If one assumes a less depleted chondritic or mantle reservoir, the relatively young T_{CHUR} ages with some very close to isochron dates would suggest a very short time lapse between the time of extraction from the various sources and the crystallization time. Relatively high $\varepsilon_{Nd2850\,Ma}$ values (−0.1 to −1.0) as opposed to some lower values (−3.2 to −3.6) and low initial $Sr_{2850\,Ma}$ ratios (0.70098–0.70314) (Table 2 and Fig. 8), indicate the importance of undepleted mantle and contribution of a slightly enriched proto-crust in the genesis of the three TTG rock types of the Sangmelima region. Given the younger zircon Pb–Pb dates for end members of the high K-granitoids or the granodioritic suite (Nédélec, 1990), reported by Tchameni et al. (2000) and Shang (2001), $\varepsilon_{Nd2650\,Ma}$ and $Sr(i)_{2650\,Ma}$ values for Sangmelima granodiorites were determined for comparison. The $\varepsilon_{Nd2650\,Ma}$ and $Sr(i)_{2650\,Ma}$ values show a greater spread than $\varepsilon_{Nd2850\,Ma}$ and $Sr(i)_{2850\,Ma}$ values. It appears then more clearly that the composition of these rocks at 2850 Ma (Fig. 8) represent closer crystallization age values than their composition at 2650 Ma.

Young Rb–Sr isochron biotite dates do portray post-crystallization thermal effects. The spread of these Paleoproterozoic dates from 2299 to 1997 Ma fall within the timing for the Eburnean orogeny and it is therefore thought that they record cooling after the thermal phase of this orogenic cycle on the Ntem complex. It should equally be noted that similar young mineral ages (biotite, amphibole, feldspars) determined using the K/Ar and Rb/Sr methods have also been reported by Lasserre and Soba (1976), Kornprobst et al. (1976) and Toteu et al. (1994).

6.3. Tectonic implications

Whereas from the chemical composition of Sangmelima TTG there appears to be no doubt as to the nature of their protolith, the formational setting remains a problem. However, the negative Nb and Ta anomaly (Fig. 6a), a characteristic of rocks derived from convergent margins could be indicative for the tectonic setting of the Sangmelima TTG. In addition, geochemical similarities between Cenozoic adakites and TTG in general (e.g. Martin, 1999; Smithies and Champion, 2000), and results obtained in this study, add more credit to ascertain the tectonic setting of these Archaean rocks. In fact, most TTG samples in this study with high Mg# (Fig. 9b), indicate that they likely interacted with the mantle wedge, hence their probable genesis by a subduction process similar to that for Cenozoic adakites. Adakites are thought to be restricted to zones where young, hot oceanic crust is subducted and partially melted at pressures high enough to stabilise garnet ± amphibole (e.g. Barker and Arth, 1976; Barker, 1979; Martin, 1986, 1999; Defant and Drummond, 1990; Beard and Lofgren, 1991; Rapp et al., 1991; Rapp, 1997). As such, it has been suggested that TTG is the Archaean equivalent of adakite (e.g. Drummond and Defant, 1990; Drummond et al., 1996; Rapp, 1997; Martin, 1999). It is therefore likely that a similar geotectonic scenario could have prevailed during the genesis of Sangmelima TTG. But could plate tectonics had operated in the same way as during recent adakitic rock production, given the supposedly homogenously mafic and dense Archaean crust? In this tectonic setting argument, it is also worth noting that compositional similarities between adakite and TTG primarily reflect only the partial melting of a similar source under similar conditions, and it has been shown that such conditions are not unique to normal subduction zones (Smithies, 2000). As such, another way to accommodate TTG composition and explain the formational context could be if subduction during the Archaean were completely flat or approximated underthrusting and locally excluded the mantle wedge (i.e. a tectonic underplating, e.g. Smithies and Champion, 2000). They noted that the compositional range of many TTG suites overlap only the low-Mg#–high-SiO_2 end of the spectrum of adakite and wedge modified adakite (case of some charnockites and granodiorites; Fig. 9), and show little if any evidence of having passed through a peridotitic mantle wedge. Flat fast subduction of young, thick and buoyant Archaean oceanic crust has equally been advocated as a significant mode of Archaean subduction by Abbott and Hoffmann (1989) and Abbott (1991).

Another alternative of a flat subduction and tectonic underplating model could have begun with thick crust formed by stacking of locally spilitized oceanic crust and/or by accretion of oceanic plateaux (e.g. $\gtrsim 35$ km; Martin, 1986; Condie, 1997; De Wit, 1998). Martin (1986) showed that the steeper geotherms in Archaean times meant that the P-T requirements for TTG production may have been commonly attained even at shallow depth. De Wit (1998), speculated that hydrated basaltic crust would yield appropriate conditions for partial melting to be achieved and low-Mg#–high-SiO_2 TTG suites would have resulted (e.g. Smithies and Champion, 2000). This model suggests that early Archaean TTG did not come into contact with the mantle (e.g. Smithies, 2000). Partial melting of hydrated basaltic material at the base of magmatically or tectonically thickened crust equally produces TTG like rocks, for instance, the Mesozoic and Cenozoic granitoids from North and South America and New Zealand (e.g. Atherton and Pertford, 1993; Muir et al., 1995; Petford and Atherton, 1996; Johnson et al., 1997), termed Phanerozoic Na-rich granitoids by Smithies (2000). The granodiorite field and a good portion of the tonalite and charnockite fields fit in the Phanerozoic Na-rich granitoid field (Fig. 9c). Sangmelima TTG therefore have features similar to those of rocks derived from both subduction and crustal thickening environments. However, the characteristic Nb and Ta negative anomalies that are peculiar signatures of subduction zones, suggest this tectonic setting as the principal scenario under which Sangmelima TTG were generated.

Besides, crustal melts would have been relatively enriched in K compared to our samples. As such, the hypothesis of a subducted basaltic crust appears much more likely (e.g. Martin, 1987a).

7. Conclusion

Sangmelima TTG are calc-alkaline I-type magmatic rocks with the tonalitic and charnockitic suites of typical trondhjemitic affinity, while granodiorites show a tendency towards the potassic calc-alkaline trend. They are aluminous ($Al_2O_3 > 15$ wt%) with $Na_2O/K_2O > 1$. Their Sm–Nd and Rb–Sr isochron data are consistent with Mesoarchaean emplacement times between ~2800 and 2900 Ma, with the three rock types crystallized from melts derived from similar late Paleoarchaean (>2.9 to ~3.2 Ga Nd T_{DM} ages) eclogite facies basaltic protocrust sources of mantle origin with slight crustal contribution in some cases, and garnet, amphibole, ilmenite and or titanite as residual phases. Similarities between Sangmelima TTG and other TTG formations worldwide in their chemical composition as well as with adakitic rocks (e.g. higher Mg# and lower SiO_2 that reflect the incorporation of a peridotitic mantle wedge component), coupled with negative Nb and Ta anomaly that is indicative of convergent margins, strongly suggest the involvement of subduction process during the formation of Sangmelima TTG. The subduction setting

could have locally been flat and excluded the mantle wedge. On the other hand, some Sangmelima TTG showing low-Mg# and high-SiO_2 composition appear to match Phanerozoic Na-rich granitoids, thought to have been generated by the melting of hydrous basaltic material at the base of or underplating thickened crust, under a typical Archaean geotherm. Given the dominantly Archaean TTG composition of the Congo craton by analogy from the composition of Ntem TTG and the characteristic negative Nb and Ta anomalies, we suggest the subduction scenario as the principal tectonic model for the genesis of the Archaean Congo craton. The effect of post-emplacement thermo-tectonic events on this craton as documented by the biotite Rb–Sr system, is related to the Eburnean orogeny.

Acknowledgments

The authors would like to thank Elmar Reitter, University of Tuebingen, for Sr and Nd isotope analyses, G. Bartholomä, and Mrs. Schuman, University of Tuebingen, for XRF analyses, and J. Navez of the Central Africa Museum, Tervuren-Belgium, for ICP-MS analyses. Constructive and thorough reviews by A. Nédélec, H. Rollinson and A.B. Kampunzu led to significant improvement of the manuscript. CKS would like to thank the Institute of Geosciences, Uni-Tuebingen, St. Paulus Parish Tuebingen and the Kreim Family-Tuebingen, for hospitality, not forgetting DAAD for the initial support in this research project.

References

Abbott, D., 1991. The case of accretion of the tectosphere by buoyant subduction. Geophysical Subduction Letters 18-4, 585–588.

Abbott, D.H., Hofmann, S.E., 1984. Archaean plate tectonics revised 1. Heat flow, spreading rate, and the age of subducting oceanic lithosphere and their effects on the origin and evolution of continents. Tectonics 3, 429–448.

Altherr, A., Henes-Klaiber, U., Hegner, E., Satir, M., Langer, C., 1999. Plutonism in the Variscan Odenwald (Germany): from subduction to collision. International Journal of Earth Sciences 88, 422–443.

Arndt, N.T., 1983. Element mobility during komatiite alteration. EOS 64, 331.

Arth, J.G., Hanson, G.N., 1975. Geochemistry and origin of the early Precambrian crust of northeastern Minnesota. Geochimica et Cosmochimica Acta 39, 325–362.

Atherton, M.P., Pertford, N., 1993. Generation of sodium-rich magmas from newly underplated basaltic crust. Nature 362, 144–146.

Barker, F., 1979. Trondhjemite. Definition, environment and hypotheses of origin. In: Barker, F. (Ed.), Trondhjemites Dacites and Related Rocks. Elsevier, Amsterdam, pp. 1–12.

Barker, F., Arth, J.G., 1976. Generation of trondhjemitic–tonalitic liquids and Achaean bimodal trondhjemites-basalt suites. Geology 4, 596–600.

Beard, J.S., Lofgren, G.E., 1991. Dehydration melting and water-saturated melting of basaltic and andesitic greenstones and amphibolites at 1, 3 and 6.9 Kbar. Journal of Petrology 32, 365–461.

Bessoles, B., Trompette, R., 1980. Géologie de l'Afrique: La Chaîne Pan-Africaine, Zone mobile d'Afrique Centrale (partie Sud) et zone Soudanaise. Mémoire BRGM N° 92.

Bickle, M.J., Bettenay, L.F., Barley, M.E., Groves, D.I., Chapman, H.J., Campbell, I.H., Laeter, J.R., 1983. A 3500 Ma plutonic and volcanic calc-alkaline province in the Archaean east Pilbara Block. Contributions to Mineralogy and Petrology 84, 25–35.

Bickle, M.J., Betternay, L.F., Chapman, H.J., Groves, D.I., McNaughton, N.J., Campbell, I.H., de Laeter, J.R., 1989. The age and origin of younger granitic plutons of the Shaw Batholith in the Archaean Pilbara Block, western Australia. Contributions to Mineralogy and Petrology 101, 361–376.

Bickle, M.J., Betternay, L.F., Chapman, H.J., Groves, D.I., McNaughton, N.J., Campbell, I.H., de Laeter, J.R., 1993. Origin of the 3500–3400 Ma calc-alkaline rocks in the Pilbara Archaean: isotopic and geochemical constraints from the Shaw batholith. Precambrian Research 60, 117–149.

Boynton, W.V., 1984. Geochemistry of the rare earth elements: meteorite studies. In: Henderson, P. (Ed.), Rare Earth Element Geochemistry. Elsevier, pp. 63–114.

Brooks, C., Wendt, I., Harre, W., 1968. A two-error regression and its application to Rb–Sr and initial Sr^{87}/Sr^{86} ratios of younger Variscan granitic rocks from the Schwarzwald Massif, Southwest Germany. Journal of Geophysical Research 73, 6071–6084.

Cahen, L., Delhal, H., Lavreau, J., 1976. The Archaean of Equatorial Africa: a review. In: Windley, B.F. (Ed.), The Early History of the Earth. Wiley, New York, pp. 486–498.

Clifford, T.N., Gass, I.G., 1970. African Magmatism and Tectonics. Olivier and Boyd, Edinburgh, 461p.

Condie, K.C., 1980. Origin and early development of the Earth's crust. Precambrian Research 11, 183–197.

Condie, K.C., 1981. Archaean Greenstone Belts. Elsevier, New York.

Condie, K.C., 1997. Contrasting sources of upper and lower continental crust: the greenstone connection. Journal of Geology 105, 729–736.

Defant, M.J., Drummond, M.S., 1990. Derivation of some modern arc magmas by melting of young subducted lithosphere. Nature 247, 662–665.

Defant, M.J., Kepezhinskas, P., 2001. Adakites: a review of slab melting and the case for a slab-melt component in arcs. In: Symposium on Adakite-like Rocks and Their Geodynamic Significance: Extended Abstracts, Beijing, China, pp. 4–7.

Delhal, J., Ledent, L., 1975. Données géochronologiques sur le complexe calco-magnésien du Sud Cameroun. Musée Royale d'Afrique Centrale (Belgium), Rapport annuel, pp. 71–75.

DePaolo, D.J., 1988. Neodymium Isotope Geochemistry, An IntroductionMinerals and Rocks, vol. 20. Springer, Berlin, Heidelberg, New York, 187p.

De Wit, M.J., 1998. On Archaean granites, greenstones, cratons and tectonics: does the evidence demand a verdict?. Precambrian Research 91, 181–226.

Drummond, M.S., Defant, M.J., 1990. A model for trondhjemite–tonalite–dacite genesis and crustal growth via slab melting: Archaean to modern comparisons. Journal of Geophysical Research 95B, 21503–21521.

Drummond, M.S., Defant, M.J., Kepezhinskas, P.K., 1996. Petrogenesis of slab-derived trondhjemite–tonalite–dacite/adakite magmas. Transactions of the Royal Society of Edinburgh: Earth Sciences 87, 205–215.

Feng, R., Kerrich, R., 1992. Geochemical evolution of granitoids from the Archaean Abitibi Southern Volcanic Zone and the Pontiac subprovince, Superior Province, Canada: implications for tectonic history and source regions. Chemical Geology 98, 23–70.

Frost, B.R., Frost, C.D., Hulsebosch, P.T., Swapp, M.S., 2000. Origin of the charnockites of the Louis Lake Batholith, Wind River Range, Wyoming. Journal of Petrology 41, 1759–1776.

Galer, S.J.G., O'Nions, R.K., 1985. Residence time of thorium, uranium and lead in the mantle with implications for mantle convection. Nature 316, 778–782.

Gill, J.B., 1981. Orogenic andesites and plate tectonics. In: Wyllie, P.J. (Ed.), Minerals and Rocks, vol. 16. Springer, Heidelberg, New York, 390p.

Goldstein, S.L., O'Nions, R.K., Hamilton, P.J., 1984. A Sm–Nd isotopic study of the atmospheric dust and particulates from major river systems. Earth and Planetary Science Letters 70, 221–236.

Goodwin, A.M., 1991. Precambrian Geology—The Dynamic Evolution of the Continental Crust. Academic Press, Harcourt Brace Jovanovich Publishers, 666p.

Green, T.H., Pearson, N.J., 1985. Experimental determination of REE partition coefficients between amphibole and basaltic to andesitic liquids at high pressure. Geochimica et Cosmochimica Acta 49, 1465–1468.

Hoffmann, P.F., 1989. Precambrian geology and tectonic history of North America. In: Bally, A.E., Palmer, A.R. (Eds.), The Geology of North America—An Overview. The Geological Society of America, pp. 447–512.

Holdaway, M.J., 1971. Stability of andalusite and the aluminium phase diagram. American Journal of Science 271, 97–131.

Irving, A.J., Frey, F.A., 1978. Distribution of trace elements between garnet megacrysts and host volcanic liquids of kimberlitic and rhyolitic composition. Geochimica et Cosmochimica Acta 42, 771–787.

Jacobson, S.B., Wasserburg, G.J., 1980. Sm–Nd isotopic evolution of chondrites. Earth and Planetary Science Letters 50, 139–155.

Jahn, B.M., Zhang, Z.Q., 1984. Archaean granulite gneisses from Eastern Hebei Province, China: Rare Earth Geochemistry and tectonic implications. Contributions to Mineralogy and Petrology 85, 224–249.

Jochum, K.P., Hofmann, A.W., Ito, E., Seufert, H.M., White, W.M., 1983. K, U and Th in mid-ocean ridge basalt glasses and heat production, K/U and K/Rb in the mantle. Nature 306, 431–436.

Johnson, K., Barnes, C.G., Miller, C.A., 1997. Petrology, geochemistry and genesis of high aluminium tonalite and trondhjemites of the Cornocorpia Stock, Blue Mountains, North-eastern Oregon. Journal of Petrology 38, 1585–1611.

Kay, R.W., Kay, S.M., 1991. Creation and destruction of lower continental crust. Geologische Rundschau 18, 259–278.

Kay, S.M., Abbruzzi, J.M., 1996. Magmatic evidence for Neogene lithospheric evolution of the central Andean "flat-slab" between 30°S and 32°S. Tectonophysics 259, 15–28.

Kay, S.M., Coira, B., Viramonte, J., 1994. Young mafic back arc volcanic rocks as indicators of continental lithospheric delamination beneath the Argentine Puna plateau, Central Andes. Journal of Geophysical Research 99 (B12), 24323–24339.

Kilpatrick, J.A., Ellis, D.J., 1992. C-type magmas: igneous charnockites and their extrusive equivalents. Transactions of the Royal Society of Edinburgh 83, 155–164.

Kornprobst, J., Lasserre, M., Rollet, M., Soba, D., 1976. Existence au Cameroun d'un magmatisme alcalin Pan-Africain ou plus ancien: la syénite néphélinique de Nkonglong. Comparaison avec les roches alcalines connues dans la même région. Bulletin Société Géologique de France 18 (5, tome XVIII), 1295–1305.

Lasserre, M., Soba, D., 1976. Age Libérien des granodiorites et des gneiss à pyroxènes du Cameroun Méridional. Bulletin BRGM 2 (4), 17–32.

Lasserre, M., Soba, D., 1979. Migmatisation d'âge Pan-Africain au sein des formations Camerounaises appartenant à la zone mobile de l'Afrique Centrale. Compte rendu sommaire. Société Géologique de France 2, 64–68.

Le Maitre, R.W., Bateman, P., Dudek, A., Keller, J., Lameyre, M.J., Le Bas, P.A., Sabine, R., Schmid, H., Sørenson, J., Streckeisen, A., Woolley, A.R., Zanettin, B., 1989. A Classification of Igneous Rocks and Glossary of Terms. Blackwell, Oxford, 193p.

Liew, T.C., Hofmann, A.W., 1988. Precambrian crustal components, plutonic associations, plate environment of the Hercynian Fold Belt of Central Europe: indications from a Nd and Sr isotopic study. Contributions to Mineralogy and Petrology 98, 129–138.

Lugmair, G.W., Marti, K., 1978. Lunar initial $^{143}Nd/^{144}Nd$: differential evolution of the lunar crust and mantle. Earth and Planetary Science Letters 39, 349–357.

Martin, H., 1986. Effect of steeper Archaean geothermal gradient on geochemistry of subduction-zone magmas. Geology 14, 753–756.

Martin, H., 1987a. Petrogenesis of Archaean trondhjemites, tonalites and granodiorites from Eastern Finland: major and trace element Geochemistry. Journal of Petrology 28, 921–953.

Martin, H., 1987b. Evolution in composition of granitic rocks controlled by time-dependence changes in petrogenetic processes: examples from the Archaean of eastern Finland. Precambrian Research 35, 257–276.

Martin, H., 1999. Adakite magmas: modern analogues of Archaean granitoids. Lithos 46, 411–429.

Martin, H., Moyen, J.-P., 2002. Secular changes in tonalite–trondhjemite–granodiorite composition as markers of the progressive cooling of Earth. Geology 30, 319–322.

Maurizot, P., Abessolo, A., Feybesse, J.L., Johan, Lecomte, P., 1986. Etude de prospection minière du Sud-Ouest Cameroun. Synthèse des travaux de 1978 à 1985. Rapport de BRGM 85, 274p.

Mpodozis, C., Cornejo, P., Kay, S.M., Titler, A., 1995. La Franja de Maricunga: Sintesis de la evolucion del Frente Volcanico Oligoceno-Mioceno de la zona sur de los Andes Centrales. Revista Geologica Chile 21, 273–313.

Muir, R.J., Weaver, S.D., Bradshaw, J.D., Eby, G.N., Evans, J.A., 1995. The Cretaceous separation point batholith, New Zealand: granitoid magmas formed by melting of mafic lithosphere. Journal of the Geological Society of London 152, 689–701.

Nédélec, A., 1990. Late calcalkaline plutonism in the Archaean Ntem unit: the Sangmelima granodioritic suite (South Cameroon). 15th Colloquium on African Geology, Publications Occasionnelle, CIFEG 22, pp. 25–28.

Nédélec, A., Nsifa, E.N., Martin, H., 1990. Major and trace element geochemistry of the Archaean Ntem plutonic complex (South Cameroon): petrogenesis and crustal evolution. Precambrian Research 47, 35–50.

Nisbet, E.G., Fowler, C.M.R., 1983. Model for Archaean plate tectonics. Geology 11, 376–379.

Norrish, K., Hutton, J.T., 1969. An accurate X-ray spectrographic method for the analyses of a wide range of geological samples. Geochimica et Cosmochimica Acta 33, 431–453.

Nsifa, E.N., Riou, R., 1990. Post Archaean migmatization in the charnockitic series of the Ntem complex, Congo craton, southern Cameroun. 15th Colloquium on African Geology, Publications Occasionnelle, CIFEG 22, pp. 33–36.

Nsifa, E.N., Tchameni, R., Belinga, S.M.E., 1993. De l'existence de formation catarchéennes dans le complexe cratonique du Ntem (Sud-Cameroun). Projet N° 273, Archaean Cratonic Rocks of Africa, Abstract volume, p. 23.

Nzenti, J.P., Barbey, P., Macaudière, J., Soba, D., 1988. Origin and evolution of the late Precambrian high-grade Yaounde gneisses (Cameroon). Precambrian Research 38, 91–109.

O'Connor, J.T., 1965. A classification of quartz rich igneous rocks based on feldspar ratios. US Geological Survey Professional Papers 525B, 79–84.

Pearce, J.A., 1983. Role of the sub-continental lithosphere in magma genesis at active continental margins. In: Hawkesworth, C.J., Norry, M.J. (Eds.), Continental Basalts and Mantle Xenoliths. Shiva, Nantwich, pp. 230–249.

Petford, N., Atherton, M., 1996. Na-rich partial melts from newly underplated basaltic crust: the Cordillera Blanca batholith, Peru. Journal of Petrology 37, 1491–1521.

Rapp, P.R., 1997. Heterogeneous source regions for Archaean granitoids. In: de Wit, M.J., Ashwal, L.D. (Eds.), Greenstone Belts. Oxford University Press, pp. 267–279.

Rapp, P.R., Watson, E.B., Miller, C.F., 1991. Partial melting of amphibolite/eclogite and the origin of Archaean trondhjemites and tonalites. Precambrian Research 51, 1–25.

Rapp, P.R., Shimizu, N., Norman, M.D., Applegate, G.S., 1999. Reaction between slab-derived melt and peridotite in the mantle wedge: experimental constraints at 3.8 GPa. Chemical Geology 160, 335–356.

Rocci, G., 1965. Essai d'interprétation des mesures géochronologiques. La structure de l'Ouest Africain. Science de la Terre France 10, 461–479.

Roddick, J.C., Sullivan, R.W., Dudás, F.Ö., 1992. Precise calibration of Nd tracer isotopic composition for Sm–Nd studies. Chemical Geology 97, 1–8.

Shang, C.K., 2001. Geology, Geochemistry and Geochronology of Archaean Rocks from the Sangmelima Region, Ntem complex, NW Congo craton, South Cameroon. Ph.D. Thesis, University of Tübingen, Germany, 313p.

Shang, C.K., Taubald, H., Satir, M., Siebel, W., Nsifa, E.N., Vennemann, T., Njilah, I.K., Ghogomu, R., 2001a. Evidence for a non-cogenetic relationship between monzogranites and TTG suite. Abstract volume EUG XI, Strasbourg, France, p. 576.

Shang, C.K., Satir, M., Siebel, W., Taubald, H., Nsifa, E.N., Westphal, M., Reitter, E., 2001b. Genesis of K-rich granitoids in the Sangmelima region, Ntem complex (Congo craton) Cameroon. Terra Nostra 5/2001, 60–63.

Sheraton, J.W., Black, L.P., 1983. Geochemistry of Precambrian gneisses: relevance for the evolution of the East Antartic Shield. Lithos 16, 273–296.

Sheraton, J.W., Collerson, K.D., 1984. Geochemical evolution of the Archaean granulite facies gneisses in the Vestfold Block and comparisons with other gneiss complexes in the Eastern Antarctic Shield. Contributions to Mineralogy and Petrology 87, 61–64.

Smithies, R.H., 2000. The Archaean tonalite–trondhjemite–granodiorite (TTG) series is not an analogue of Cenozoic adakite. Earth and Planetary Science Letters 182, 115–125.

Smithies, R.H., Champion, D.C., 2000. The Archaean high-Mg diorite suite: links to tonalite–trondhjemite–granodiorite magmatism and implications for early Archaean crustal growth. Journal of Petrology 41, 1653–1671.

Smithies, R.H., Champion, D.C., Cassidy, K.F., 2003. Formation of Earth's early Archaean continental crust. Precambrian Research 127, 89–101.

Spear, F.S., 1993. Metamorphic Phase Equilibra and Pressure–Temperature–Time Paths. Mineralogical Society of America, Washington, 799p.

Steiger, R.H., Jäger, E., 1977. Subcommision on geochronology: conventions of the use of decay constants in geochronology and cosmochronology. Earth and Planetary Science Letters 36, 359–362.

Sun, S.S., McDonough, W.F., 1989. Chemical and isotopic systematics of oceanic basalts: implications for mantle composition and processes. In: Saunders, A.D., Norry, M.J. (Eds.), Magmatism in Ocean Basins. Geological Society of London. Special Publications 42, 313–345.

Tarney, J., Dalziel, I.W.D., De Wit, M.J., 1976. Marginal basin rocas verdes complex from southern chile: a model for Arhaean greenstone belt formation. In: Windley, B.F. (Ed.), The Early History of the Earth. Wiley, London, pp. 131–146.

Tchameni, R., 1997. Géochimie et géochronologie des formations de l'Archéen et du Paléoprotérozoïque du Sud-Cameroun (Groupe du Ntem, Craton du Congo). Thèse de l'Univérsité d'Orléans, France, 356p.

Tchameni, R., Mezger, K., Nsifa, N.E., Pouclet, A., 2000. Neoarchaean evolution in the Congo craton: evidence from K rich granitoids of the Ntem complex, southern Cameroon. Journal of African Earth Sciences 30, 133–147.

Tchameni, R., Mezger, K., Nsifa, N.E., Pouclet, A., 2001. Crustal origin of Early Proterozoic syenites in the Congo craton (Ntem complex), South Cameroon. Lithos 57, 23–42.

Toteu, S.M., Van Schmus, W.R., Penaye, J., Nyobe, J.B., 1994. U–Pb and Sm–Nd evidence for Eburnean and Pan-African high grade metamorphism in cratonic rocks of southern Cameroon. Precambrian Research 67, 321–347.

Vicat, J.P., Leger, J.M., Nsifa, E., Piguet, P., Nzenti, J.P., Tchameni, R., Pouclet, A., 1996. Distinction au sein du craton congolais du Sud-Ouest du Cameroun, de deux épisodes doléritiques initiant les cycles orogéniques éburnéen (Paléoprotérozoïque) et Pan-Africain (Néoprotérozoïque). Compte Rendu de l'Académie des Sciences, série IIa 323, 575–582.

Wendt, I., 1986. Radiometrische Methoden in der Geochronologie. Clausthaler Tektonische Hefte 23. Pilger Verlag, 170p.

White, A.J.R., Chappell, B.W., 1977. Ultrametamorphism and granitoid genesis. Tectonophysics 43, 7–32.

Windley, B.F., 1976. New tectonic models for the evolution of Archaean continents and oceans. In: Windley, B.F. (Ed.), The Early History of the Earth. Wiley, New York, pp. 105–112.

Yogodzinski, G.M., Kay, R.W., Volynets, O.N., Koloskov, A.V., Kay, S.M., 1995. Magnesian andesite in the western Aleutian Komandorsky region: implications for slab melting and processes in the mantle wedge. Geological Society of America Bulletin 107, 505–519.